Journal of Neurochemistry

WILEY

Journal of Neurochemistry JNC The Official Journal of the International Society for Neurochemistry

ORIGINAL ARTICLE OPEN ACCESS

Altered Mitochondrial Bioenergetics and Calcium Kinetics in Young-Onset *PLA2G6* Parkinson's Disease iPSCs

Thasneem Musthafa[1] | Syed Kavish Nizami[1] | Ankita Mishra[2] | Gaiti Hasan[1,3] | Renjitha Gopurappilly[1,2]

[1]National Centre for Biological Sciences, Tata Institute of Fundamental Research, Bangalore, India | [2]NKure Therapeutics Pvt Ltd, Centre for Cellular and Molecular Platforms, Bangalore, India | [3]Centre for High Impact Neuroscience and Translational Applications, Kolkata, India

Correspondence: Gaiti Hasan (gaiti@ncbs.res.in) | Renjitha Gopurappilly (renjitha@nkure.com; renjithap@ncbs.res.in)

Received: 28 June 2024 | **Revised:** 17 March 2025 | **Accepted:** 19 March 2025

Funding: This study was supported by The Wellcome Trust DBT India Alliance, IA/E/18/1/504319.

Keywords: disease modeling | human iPSC | mitochondrial dysfunction | Parkinson's disease | PLA2G6

ABSTRACT

Parkinson's disease (PD) has emerged as a multisystem disorder affecting multiple cellular and organellar systems in addition to the dopaminergic neurons. Disease-specific induced pluripotent stem cells (iPSCs) model early developmental changes and cellular perturbations that are otherwise inaccessible from clinical settings. Here, we report the early changes in patient-derived iPSCs carrying a homozygous recessive mutation, R741Q, in the *PLA2G6* gene. A gene-edited R747W iPSC line mirrored these phenotypes, thus validating our initial findings. Bioenergetic dysfunction and hyperpolarization of mitochondrial membrane potentials were hallmarks of the PD iPSCs. Further, a concomitant increase in glycolytic activity indicated a possible compensation for mitochondrial respiration. Elevated basal reactive oxygen species (ROS) and decreased catalase expression were also observed in the disease iPSCs. No change in autophagy was detected. These inceptive changes could be potential targets for early intervention of prodromal PD in the absence of disease-modifying therapies. However, additional investigations are crucial to delineate the cause-effect relationships of these observations.

1 | Introduction

Mutations in calcium-independent phospholipase A2 group VI (*PLA2G, iPLA2β, PARK14*) are associated with neurodegenerative disorders (PLA2G6-associated neurodegeneration-PLAN) such as infantile neuroaxonal dystrophy (INAD), Atypical neuroaxonal dystrophy (ANAD), PLA2G6-related dystonia-parkinsonism, and autosomal recessive early-onset Parkinsonism (AREP) (Gregory et al. 1993). The *PLA2G6* variants are rare, with high penetrance causing atypical Parkinson's disease (PD) (Cova and Priori 2018). PLA2G6 protein produces free fatty acids and lysophospholipids by hydrolyzing the sn-2 ester bonds of the membrane glycophospholipids. The PLA2G6 protein has two distinct isoforms-85kD (VIA-I) and 88kD (VIA-II) in addition to many N-terminal truncated forms generated by alternative splicing and proteolytic cleavage. The protein contains an N-terminal, ankyrin repeats, GXSXG lipase catalytic site, nucleotide-binding domain, calmodulin-binding domain, and C-terminal (Figure 1A) (Tang et al. 1997; Wolf and Gross 1996). There are 15 different mutations associated

Abbreviations: ANAD, atypical neuroaxonal dystrophy; AREP, autosomal recessive early-onset Parkinsonism; BAF A, bafilomycin A; CRISPR, clustered regularly interspaced short palindromic repeats; DA, dopamine; DCFDA, 2′,7′-dichlorodihydrofluorescein diacetate; ECAR, extracellular acidification rate; ER, endoplasmic reticulum; ETC, electron transport chain; FCCP, carbonyl cyanide 4-(trifluoromethoxy) phenylhydrazone; INAD, infantile neuroaxonal dystrophy; IP_3R, inositol 1,4,5-trisphosphate receptor; IPD, idiopathic Parkinson's disease; iPSC, induced pluripotent stem cells; LC3, microtubule-associated protein 1A/1B-light chain 3; MCU, mitochondrial calcium uniporter; NAC, N-acetyl-L-cysteine; OA, orai activator; OCR, oxygen consumption rate; OMM, outer mitochondrial membrane; OXPHOS, oxidative phosphorylation; PBMC, peripheral blood mononuclear cells; PD, Parkinson's disease; PLAN, PLA2G6- associated neurodegenerative disorders; PM, plasma membrane; ROS, reactive oxygen species; RRID, Research Resource Identifier; SERCA, sarcoendoplasmic reticulum calcium ATPase; SNP, single nucleotide polymorphism; SNpc, substantia nigra pars compacta; SOCE, store-operated calcium entry; SRC, spare respiratory capacity; STIM, stromal interaction molecule; TMRE, tetramethylrhodamine, ethyl ester; VDAC, voltage-dependent anion channels.

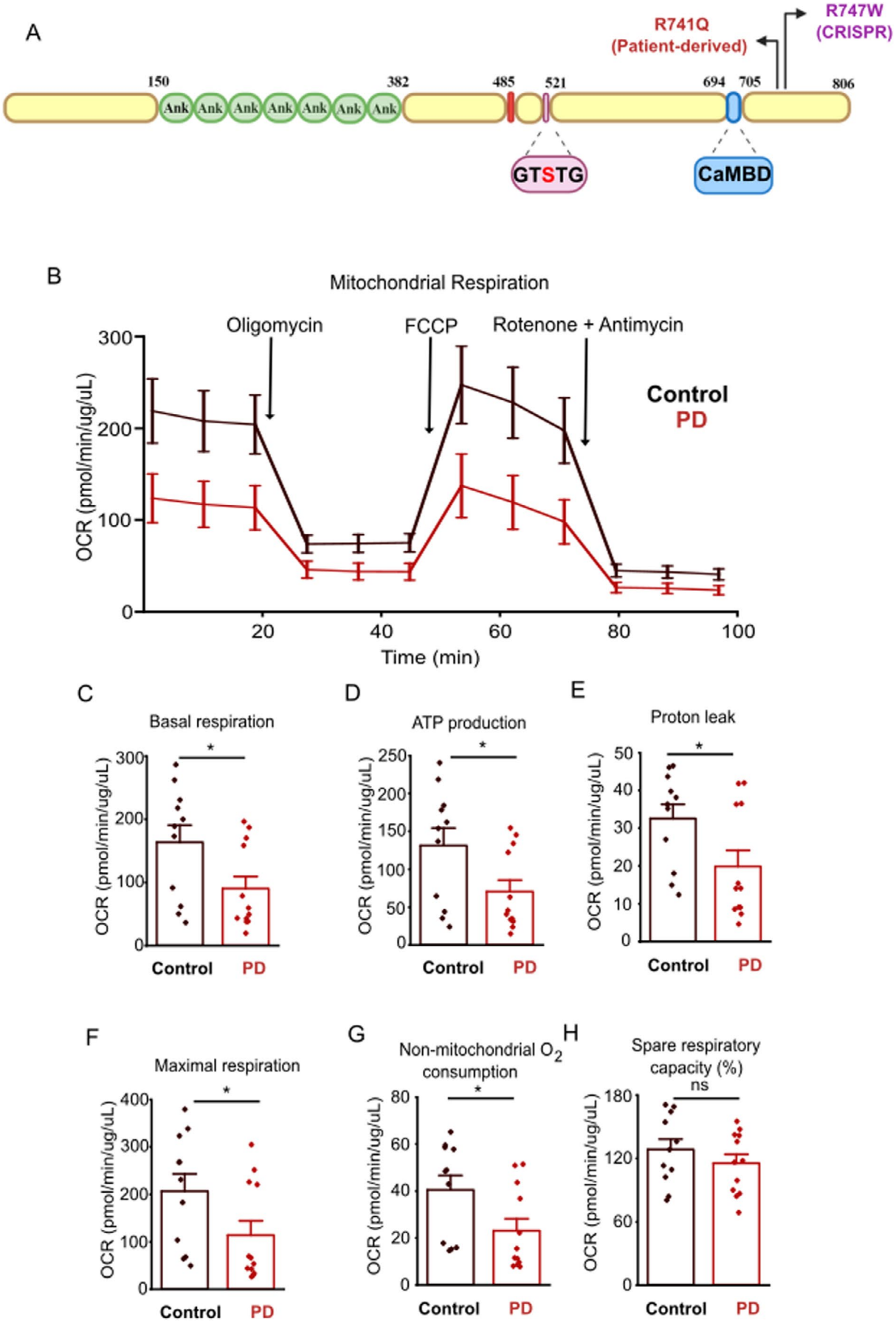

FIGURE 1 | Legend on next page.

FIGURE 1 | PLA2G6–R741Q iPSCs show impaired mitochondrial respiration. (A) Schematic representation of functional domains of PLA2G6 protein with the R741Q and R747W mutation sites—seven ankyrin domains marked as Ank (between amino acids 150–382), a glycine-rich nucleotide-binding domain (red oval shape, centred at amino acid 485), GTSTG lipase catalytic domain with the serine active site (S519) highlighted in light red (pink oval shape, amino acids 517–521), calmodulin-binding domain marked as CaMBMD (blue oval shape, amino acids 747–759). The locations of mutations are R741Q, present in the patient-derived iPSCs (red) and R747W in the CRISPR-engineered iPSCs (purple); (B) representative average trace of mitochondrial respiration of PLA2G6-R741Q PD iPSCs (PD, red) and its familial control-derived iPSCs (Control, black) from Seahorse mitochondrial stress assay (n=3 independent cell culture preparations, Control iPSC-11 assay wells, PD iPSC-12 assay wells). The time of addition of oligomycin, FCCP, rotenone, and antimycin is marked with black arrows; (C) rate of basal oxygen consumption; (D) rate of ATP production; (E) rate of proton leak; (F) rate of maximal respiration; (G) rate of non-mitochondrial oxygen consumption; (H) spare respiratory capacity. (B-H) represented as mean ± SEM after normalization with protein content. Each dot represents a Seahorse assay plate well, Shapiro–Wilk test was done to determine normality of the distribution, Mann-Whitney U test $*p < 0.05$, ns-non-significant ($p \geq 0.05$). OCR-oxygen consumption rate. Color codes: PD-Patient-derived iPSCs with R741Q (Red), Control-familial control-derived iPSCs (Black).

with PLA2G6-associated adult-onset dystonia-parkinsonism (Gopurappilly 2021). The single nucleotide mutations c.2222G>A (R741Q) and c.2239C>T (R747W) were the first mutations reported and characterized. The mutations associated with PLA2G6-related dystonia-parkinsonism have normal PLA2G6 enzyme catalytic activity, unlike mutations related to other PLAN disorders (Engel et al. 2010).

Several links to mitochondrial dysfunction have been described in idiopathic (IPD) and monogenic PD caused by dominant and recessive mutations. However, mitochondrial defects are directly implicated in recessive PD pathology and are reported across PD models with mutations in *PINK1* and *Parkin* (Henrich et al. 2023; Scorziello et al. 2020; Zanellati et al. 2015). The mechanisms underlying autosomal recessive PD (Gopurappilly 2021) and the role of mitochondria in neurodegeneration (Grünewald et al. 2019) are reviewed earlier and are beyond the scope of this study. The reports on the less studied recessive *PLA2G6* mutations, relevant to our findings, are discussed herein. Various studies in *Drosophila* with loss of PLA2G6 exhibit mitochondrial and lysosomal dysfunction, increased lipid peroxidation, and elevated oxidative and ER stress, leading to impaired neuronal activity (Iliadi et al. 2018; Kinghorn et al. 2015; Mori et al. 2019). Similarly, mitochondrial and ER stress and autophagic impairment were observed in a rodent knock-in model with D331Y *PLA2G6* mutations accompanied by degeneration of dopaminergic (DA) neurons of substantia nigra pars compacta (SNpc) (Chiu et al. 2017). Ca^{2+} dyshomeostasis is another key feature of neurodegenerative disorders and, in particular, PD. The change in intracellular calcium (Ca^{2+}) levels signals differential gene expression relevant to cell health and apoptosis. The fly orthologue of the *PLA2G6* gene, *CG6718*, was identified as a SOCE (store operated Ca^{2+} entry) modulator (Vig et al. 2006). Furthermore, in vitro studies on cell lines with mutations in *PLA2G6*, such as primary fibroblasts from patients with R747W and patient-derived DA neurons with D331Y, have shown decreased SOCE (Ke et al. 2020; Zhou et al. 2016). A recent study on mitochondrial Ca^{2+} dysregulation and ER Ca^{2+} replenishment in GBA-N370S iPSC-dopamine neurons described a reduction in PLA2G6 protein level and ER-mitochondria proximity (Beccano-Kelly et al. 2023).

Patient-derived induced pluripotent stem cells (iPSC) and cell lines derived from them (neural precursor cells, dopaminergic neurons, microglia) are promising in vitro models to characterize the molecular and cellular changes in various neurodegenerative models. While some of these are evident from the undifferentiated or iPSC stage, some changes only become apparent over the differentiation trajectory, and hence only in certain cell types. It is important to consider that the stage at which these molecular changes become detectable depends on multiple factors, including the mutations that lead to the PD pathology. For instance, mitochondrial dysfunction and an increase in oxidative stress were seen in *PARK2* iPSC-derived neurons, but fibroblasts or iPSCs did not exhibit these changes (Imaizumi et al. 2012). In contrast, mitochondrial dysfunction was evident in fibroblasts with *PARK2* mutations in another study (Zanellati et al. 2015). Such observations date back to decade-long analyses from peripheral cells of PD patients where compromised mitochondrial function has been reported in IPD (Mytilineou et al. 1994; Winkler-Stuck et al. 2004) and *PINK1* PD (Morais et al. 2014; Rakovic et al. 2010; Rothfuss et al. 2009).

For a long time, PD was treated as a neurodegenerative movement disorder with very little or no emphasis on changes happening in other organs or tissue types. With the advent of multiple omics profiling techniques and open data sources, there is more evidence of manifestations of phenotypic changes in cell types other than neurons in PD, such as peripheral mononuclear cells (PBMC) and fibroblasts (Hekselman and Yeger-Lotem 2020). Characterizing the non-motor autonomic physiological symptoms in various organ and tissue systems would enable early detection of PD and therapeutics for better symptom management and increasing the life quality of patients. Here, we report that patient-derived iPSC with R741Q mutations in the *PLA2G6* gene exhibits early signs of mitochondrial dysfunction and Ca^{2+} dyshomeostasis. Further, we validate our results using a CRISPR-engineered isogenic iPSC line with R747W mutation in *PLA2G6*. Similar results from these two iPSC lines indicate these defects are largely mutation-driven. This study also validates the hypothesis that PD is a multiorgan disorder as the phenotypes can be observed in 'non-disease relevant cells'. These non-neuronal cell types can be targeted for early diagnosis and high throughput screening studies. Together, we propose that such iPSC lines are useful models to study *PLA2G6*-associated PD and associated cellular and molecular changes.

2 | Materials and Methods

2.1 | Cell Culture

The study was approved by the Institutional Ethics Committee of National Centre for Biological Sciences (NCBS/IEC-10/001). Informed consent forms were obtained from the patient and the parent. Human induced pluripotent stem cells (hiPSCs) were derived from a *PLA2G6* PD patient (R741Q) and an unaffected parent as described earlier (Gopurappilly et al. 2023). The undifferentiated iPSC colonies were maintained in Stemflex media (Thermo Fisher Scientific, Cat# A3349401) on hESC-grade matrigel (Corning, Cat# 354277) and passaged every 5–6 days using 1X EDTA solution (Sigma-Aldrich, Cat# E8008). RevitaCell supplement (Thermo Fisher Scientific, Cat# A2644501) was added on the day of thawing. The R741Q patient iPSC line was termed "PD" and the familial control "CONTROL" for easy interpretation. Both lines were passage-matched for the functional assays and other experiments. For validation experiments, CRISPR-edited iPSCS with R747W mutation in the PLA2G6 loci and its isogenic control were used (Synthego, CA). These cells were designated as MUTANT and WILD TYPE (WT) to differentiate them from the patient cells. All experiments were done with the R741Q iPSCs between passages 18–23, and CRISPR-edited iPSCS were between passages 38–45. The culture media and passage conditions were similar to the in-house-derived iPSCs. Cells were grown in a 37°C humidified incubator with 5% CO_2 in normoxic conditions. For long-term storage, cells were cryopreserved in CryostorCS10 (Stem Cell Technologies, Cat# 07959) or CTS PSC Cryomedium (Thermo Fisher Scientific, Cat# A4239301) and banked in liquid nitrogen storage tanks.

2.2 | Seahorse Assay

Both mitochondrial stress assays (oxygen consumption rate, OCR) and glycolytic stress assays (extracellular acidification rate, ECAR) were performed using the Agilent Seahorse XFe24 system (RRID:SCR_019539) as per general manufacturer's instructions. Cells were plated 24 h before the day of the assay. The cartridges were kept for overnight hydration in an XF Calibrant solution inside a 37°C non-CO_2 incubator. The cartridges were taken out 1 h before the assay, and the injection ports were loaded with chemicals according to the protocol.

The wells for mitochondrial stress assay were washed twice with the assay buffer (pH 7.4) containing glucose (10 mM), L-glutamine (2 mM), and sodium pyruvate (1 mM). A final volume of 500 μL of assay buffer was added, and the plate was kept at 37°C for an hr. before the experiment. A final well concentration of 1 μM of oligomycin (Sigma-Aldrich, Cat# 75351), 1 μM FCCP (Sigma-Aldrich, Cat# C2920), and 0.5 μM of rotenone and antimycin mixture in the assay buffer were loaded to ports A, B, and C of the cartridge, respectively. For glycolytic stress assays, the cells were washed with the assay buffer containing 2 mM L-glutamine at pH 7.4. The cartridge wells were loaded with assay chemicals dissolved in the buffer to a final well concentration of 10 mM glucose, 1 μM oligomycin, and 50 mM 2-deoxyglucose (2-DG) to inject ports A, B, and C, respectively. All the reagents were purchased from Agilent Technologies as part of the assay kits. The proteins were eluted by adding RIPA (Sigma-Aldrich) with a protease inhibitor cocktail (Sigma-Aldrich) to each well. Protein concentration was quantified using a BCA assay kit (Thermo Fisher Scientific) by a Varioskan multimode reader. The readings were normalized to the total protein content of each well. The outliers were removed, and the data was exported to Excel using the Wave Controller software (RRID:SCR_024491).

2.3 | Calcium Imaging

2.3.1 | SOCE

Cells were grown on commercially available imaging dishes as monolayers. The cells were incubated with 4 μM Fura-2 AM (Invitrogen, Cat# F1221) and 20% Pluronic F-127 (Sigma-Aldrich, Cat# P2443) in culture media for 40 min at RT. The cells were washed twice with the media and kept in fresh media until it was used for imaging. The imaging paradigm and analysis to assess the SOCE were done as described earlier by (Gopurappilly et al. 2019). The number of frames was increased to 250 following the addition of thapsigargin (TG, Invitrogen, Cat# T7458) and calcium chloride (Sigma-Aldrich, Cat# 449709) to accommodate the extended response by the iPSC cells. To obtain the maximal fluorescence ratio (R_{max}) and minimum fluorescence under 380 nm excitation, corresponding to R_{max} ($F380_{min}$), 1 mM ionomycin (Calbiochem, Cat# 407950) was added. The minimal fluorescence ratio (R_{min}) and the maximum fluorescence with 380 nm ($F380_{max}$) were calculated using 15 mM EGTA (Sigma-Aldrich, Cat# E3889) with 0.05% TritonX-100 (Sigma-Aldrich, Cat# 93443). Image acquisition was performed using the Andor iXON 897E EMCCD camera and AndoriQ 2.4.2 imaging software (RRID:SCR_014461). The values used for conversion of the F340/F380 ratio to the concentration of calcium were the average of these parameter values obtained from more than 5 plates for each group. Basal calcium levels were calculated for each cell by taking the average of the first 25 frames in the Ca^{2+}-free HBSS. Store release and SOCE were calculated as the difference between the maximal point and basal calcium levels after the addition of thapsigargin (TG) and calcium chloride, respectively. The rate of SOCE is the first-order differential of the response from $t = 550$ to 700 s.

2.3.2 | Mitochondrial Calcium Imaging

The mitochondrial calcium release was imaged using Rhod-2 AM (Invitrogen, Cat# R1245MP). The cells were co-stained with Fluo-4 AM (Invitrogen, Cat# F14201) to look at the changes in cytoplasmic calcium as a result of mitochondrial calcium. The cells were grown on imaging dishes and incubated with culture media containing 4 μM Fluo-4 AM, 4uM Rhod-2 AM and 20% of Pluronic acid (Sigma-Aldrich) at RT for 40 min. Two washes were given using fresh media for 15 min each. The imaging was done using a Zeiss LSM 980 Airyscan setup (RRID:SCR_025048) with altering 488 and 561 channels at an interval of 1.04 s. The media was changed to calcium HBSS (same composition used

for SOCE imaging) immediately before imaging each plate. The first 25 frames were imaged for basal calcium levels. After that, 5 μM FCCP (Sigma-Aldrich, Cat# C2920) in Ca^{2+} free HBSS was added to depolarize the mitochondria and release the calcium from them. All images were subjected to Airyscan processing using the ZEN 3.8 desktop software and analyzed using FIJI—Image J (RRID:SCR_003070). The whole cells were used as regions of interest for both dyes and marked using the Fluo-4 AM staining (488 channel). The ratios were obtained from 8-bit images. The raw fluorescence ratios were normalized using the average of fluorescence from basal frames using the equation- $\frac{\Delta F}{F\text{Basal}} = \frac{F - F\text{Basal}}{F\text{Basal}}$. The maximal calcium release from each cell was determined by the difference between the basal normalized fluorescence and the minimal fluorescence after the addition of the FCCP. The percentage difference in the fluorescence from the basal mitochondrial potential was calculated as $\left(\frac{F}{F\text{Basal}} \times 100\right)$.

2.4 | Mitochondrial Membrane Potential

The mitochondrial membrane potential was assessed using the dye-Tetramethylrhodamine, Ethyl Ester (TMRE, Invitrogen, Cat# T669). The cells were stained with Fluo-4 AM (Invitrogen, Cat# F14201) to mark the cell boundaries. The cells were seeded at least 48 h prior to the imaging. The cells were incubated with 4 μM Fluo-4 AM and 20% Pluronic acid (Sigma-Aldrich) in culture media for 40 min at RT. Two washes were done using fresh media to remove the extra dye and for desertification for 10 min each. Images were acquired using a Zeiss LSM 980 Airyscan setup (RRID:SCR_025048) . Each plate was incubated with TMRE in culture media for 30 min just before the imaging—20 min incubation and two 10 min washes with fresh media. The imaging was done using the Airyscan mode with altering 480 and 561 nm channels at an interval of 1.04 s. The imaging was done in the HBSS buffer with calcium. The first 25 frames were used as an acclimatization period, and the subsequent 25 frames were used to establish the baseline. 5 μM FCCP (Sigma-Aldrich, Cat# C2920) in HBSS was added to look at the change in membrane potential after the depolarization. All images were subjected to Airyscan processing, and the ROIs were made inside the plasma membrane (the dye stains the plasma membrane as it is cationic) to avoid their contribution. The ratios were obtained from 8-bit images using FIJI- Image J (RRID:SCR_003070) and normalized using the following equation: The ratios were obtained from 8-bit images. The raw fluorescence ratios were normalized using the average of fluorescence from basal frames using the equation- $\frac{\Delta F}{F\text{Basal}} = \frac{F - F\text{Basal}}{F\text{Basal}}$.

2.5 | Basal Mitochondrial ROS

To qualitatively compare the basal levels of ROS, 2′,7′-dichl orodihydrofluorescein diacetate (H_2DCFDA, Thermo Fisher Scientific, Cat# D399) was used. The stock solutions were prepared in ethanol. A final concentration of 1 μM/μL in 1× DPBS was used to incubate the cells for 30 min inside an incubator (37°, 5% CO_2). The plates were washed with 1× DPBS twice for 10 min each and imaged immediately after that. The Z-stacks of cells were imaged using an Olympus FV3000 using the 488 nm channel. The images were Z-projected using FIJI-Image J (RRID:SCR_003070) using the maximum project method. Whole cells were considered as ROIs, and the fluorescence readings were plotted using Origin (RRID:SCR_014212). 5 biological replicates were considered for each genotype for the comparison. Cells were treated with 10 mM N-acetyl-L-cysteine (NAC Sigma- Aldrich, Cat# A7250) for 3 h prior to loading them with H2DCFDA as a control to quench ROS. Cells were washed with 1× DPBS twice for 5 min each before dye loading. The Shapiro–Wilk test was done to check the normality of the distribution, and the Mann–Whitney test was used to calculate the significance level. The NAC controls were not quantified as the fluorescence was quenched, resulting in a poor signal.

2.6 | Immunoblotting

For LC3B blots, cells were grown in 6-well plates and treated with 50 μM Bafilomycin A (Sigma-Aldrich, Cat# B1793) or with DMSO (vehicle, Sigma-Aldrich, Cat# 276855) for 20 h. Proteins were eluted in RIPA buffer with a protease inhibitor cocktail. Protein concentration was obtained using a standard BCA assay (Pierce BCA Protein Assay kit, Thermo Fisher Scientific, Cat# 23225) with a Varioskan multimode reader. 50 μg proteins were loaded with a 4× Laemmli buffer after denaturing for 5 min at 95°C. 1.5 mm 14% SDS gels were used to separate the LC3BI (16kD) and LC3BII (14kD). 2 μM PVDF was activated using methanol for 15 min. The gel, Whatman filter papers, and activated PVDF were kept in a 1× transfer buffer for 15 min for better transfer efficiency. The gels were transferred for 20 min at 20 V using a TransBlot semidry transfer system (BioRad). The blots were blocked by incubating with 5% bovine serum albumin (BSA) in 1× TBST for 1 h at RT on a rocker. The blots were later incubated with primary antibodies overnight with low rocking. A mix of diluted primary antibodies-LC3B (1:1000, Cell Signaling Technology, Cat# 3868) and β-Tubulin (1:3000, DSHB E7, Cat# AB_2315513, RRID:AB_528499) was made using fresh 5% BSA in 1× TBST. The blots were washed in 1× TBST for 10 min thrice at high-speed rocking. The blots were later incubated with secondary antibodies conjugated with HRP for 1 h at RT on a rocker. Blots were imaged using a Pierce ECL Western Blotting Substrate (Thermo Fisher Scientific) in an ImageQuant LAS 4000 GE system using a multiple exposure program with ImageQuant software (RRID:SCR_014246). The bands were quantified using FIJI-ImageJ (RRID:SCR_003070) in 8-bit format. A paired test with a 0.05 significance level was used.

For the STIM blots, the proteins were eluted using RIPA and ran similarly to the LC3B blots except for the following steps. A 1.5 mm, 8% SDS gel was used for running the samples. 30 μg proteins were loaded for each sample and ran at room temperature. The blot was transferred using the semidry system at 15 V for 15 min. The blots were incubated with STIM1antobody (Cell Signaling Technology, Cat# 5668S, RRID:AB_10828699) and β-Tubulin (1:3000, DSHB E7, Cat# AB_2315513, RRID:AB_528499) overnight. Secondary antibodies used for the blots were anti-mouse HRP (1:3000; Cell Signaling Technology Cat# 7076, RRID:AB_330924) and anti-rabbit HRP (1:3000; Thermo Fisher Scientific Cat# 32260,

RRID:AB_1965959). A student's t-test was used to obtain the significant difference.

2.7 | Immunofluorescence

To monitor autophagic flux in single cells, RFP-GFP-LC3 tandem construct (ptfLC3 Cat #21074, RRID:Addgene_21074) was electroporated into the iPSC cells with the Neon Electroporation System (Invitrogen) at 1200 V and two pulses of 20 ms width. This plasmid enables differential detection of autophagosomes as yellow puncta (signals of both RFP and GFP) and autolysosomes as red puncta (only RFP signal as GFP signal is quenched by acidic lysosomal pH). The cells were treated with Bafilomycin A or DMSO as explained earlier and fixed in 4% paraformaldehyde. Images were captured using Olympus FLUOVIEW FV4000 microscope under the 60× oil objective. ImageJ software (RRID:SCR_003070) was used for quantification after background subtraction and manual thresholding.

2.8 | RT-qPCR

The RNA extraction was performed using the standard TRIzol method. The purity and concentration of RNA samples were checked using a NanoDrop spectrophotometer (Thermo Fisher Scientific, RRID:SCR_018042). Prior to the cDNA synthesis, DNase treatment was performed. A reaction mixture of 1 μg isolated RNA with a cocktail of 0.5 U DNAse I (amplification grade), 1 mM DTT, 20 U of RNase inhibitor (RNase OUT), and ultrapure water (to make it up to 22.5 μL) was made for each sample. These reaction mixtures were incubated at 37°C for 30 min and heat-inactivated at 70°C for 10 min using a thermocycler (Eppendorf). The cDNAs were synthesized using 200 U of Moloney murine leukemia virus (MMLV) reverse transcriptase, 50 μM random hexamers, and 1 mM deoxyribonucleotide triphosphate (dNTPs) using a thermocycler (Eppendorf). All the reagents were purchased from Thermo Fisher Scientific unless specified otherwise.

The fold change in gene expression was obtained by doing real-time—quantitative PCRs (RT-qPCRs). A fast protocol was performed using the ABI 7500 Fast machine (Applied Biosystems, RRID:SCR_019334) in a 96-well setup. Each reaction mixture was of 10 μL, prepared by mixing 100 nM forward and reverse primers of the gene of interest and the KAPA SYBR FAST reagent (Sigma-Aldrich, Cat# SF1UKB). The fold changes were calculated using the double delta C_t analysis method. The primer details are given in Table 1.

Cells were treated with 10 mM N-acetyl-L-cysteine (NAC) for 3 h to check for the rescue of the catalase gene expression and were subjected to RT-qPCR as described.

2.9 | Statistical Analysis

In all cases, the normality of the distribution was checked using the Shapiro–Wilk test. Student's t-tests were used for normal distributions, and Mann–Whitney U tests were used for non-normal distributions to assess the significance (unless mentioned otherwise in the methods). No test for outliers was conducted. Two-tailed t-tests (two-sample) was used for direct comparison in all analyses. Western blot analysis was performed using paired t-test. All plots and analyses were done using the Origin Pro Student's version (RRID:SCR_014212). The significance levels are indicated by asterisks: $*p<0.05$, $**p<0.01$, $***p<0.001$. The statistical details of experiments can be found in the Figure legends. Final figures were made in Inkscape (RRID:SCR_014479). Schematic figures were created with Biorender (RRID:SCR_018361).

3 | Results

3.1 | Mitochondrial Respiration Is Impaired in iPSCs with Point Mutations in the *PLA2G6* Gene, Causing Early-Onset Parkinsonism

The identification of early disease signs in PD can help understand the onset, considering that a long prodromal stage is invariably present in all cases. Dysfunctional mitochondrial respiration has been associated with sporadic and familial PD (Henrich et al. 2023; Palacino et al. 2004; Risiglione et al. 2021; Scorziello et al. 2020; Zanellati et al. 2015). These changes are reported consistently from postmortem clinical samples to iPSC-derived dopaminergic neurons (Beccano-Kelly et al. 2023; Henrich et al. 2023; Imaizumi et al. 2012; Scorziello et al. 2020). We used the Seahorse-based mitochondrial stress assay to assess if mitochondrial respiration is affected in the PD cells with an R741Q mutation in the *PLA2G6* gene. The overall respiratory responses of the patient-derived iPSCs as compared to their familial control cells are plotted as OCR (Figure 1B). The serial addition of various drugs, ATP synthase inhibitor oligomycin, electron transport chain (ETC) uncoupler FCCP, and a mixture of complex I and III inhibitors rotenone and antimycin A in the program are indicated.

Patient-derived iPSCs showed lower mitochondrial respiration than control cells under basal conditions (Figure 1C). Basal respiration is contributed to by respiration associated with proton leak and ATP production. The patient-derived cells also exhibited a significant reduction in ATP production (Figure 1D) and proton leak (Figure 1E). Basal respiration can also be linked to the transport of Ca^{2+} or other ions across the mitochondrial membrane and, therefore, the mitochondrial membrane potential (Divakaruni et al. 2014). The patient iPSCs showed a change in these mitochondrial parameters (Figures 3 and 4) and are discussed subsequently.

FCCP uncouples the mitochondrial proton gradient and pushes the ETC toward its maximal activity. It is tightly linked to the energy needs of the cells under physiological conditions. The patient-derived cells exhibit a decrease in maximal respiration (Figure 1F) and non-mitochondrial oxygen consumption (Figure 1G). Maximal respiration is the maximum capacity that the electron respiratory chain can reach, whereas non-mitochondrial respiration is the oxygen consumption due to cellular enzymes after injection of rotenone and antimycin A. The difference between maximal and basal respiration, known as the spare respiration, was not significantly different

TABLE 1 | Details of primers.

Sl No	Gene	Sequence
1	MCU	ACGGTACACCAGAGGATCGC (F)
		TGAGTGTGAACTGACAGCGTT (R)
2	TMEM65	TGCTGCTTTGGGAAATCTTGTG (F)
		CTTGCTTTGGTGTGAGATCAGGAA (R)
3	MICU1	ACTGTGATGGCAATGGCGAA (F)
		TAAAGCGAAGTCCCAGGCAG (R)
4	MICU2	AGAGACCTTGGCGATAAAGGG (F)
		ATCCAGAATGGGGTTTAGTGAGG (R)
5	MCUB	AGAAGCTCATTCGGAAGCCAA (F)
		CCAGGAGTACACCCACCAC (R)
6	MCUR1	ATGCCTTAGTGTGCTTACTGGA (F)
		TTCACATTCGCAATCTGAGACAT (R)
7	EMRE	ATTTTGCCCAAGCCGGTGAA (F)
		CCTCAAGCAGAGCAGCGAAG (R)
8	SLC25A23	TGAAGAACTGGTGGCTTCAG (F)
		TGCTCACAGCTGGAATAACCT (R)
9	NCLX	CCGGCAGAAGGCTGAATCTG (F)
		ACCTTGCGGCAGTCTACCAC (R)
10	SOD1	GGTGGGCCAAAGGATGAAGAG (F)
		CCACAAGCCAAACGACTTCC (R)
11	SOD2	CCAAATCAGGATCCACTGCAA (F)
		CAGCATAACGATCGTGGTTTACTT (R)
12	CAT	TCCAAGGCAAAGGTATTTGAGCA (F)
		CAACGAGATCCCAGTTACCATCTTC (R)
13	STIM1	CACACTCTTTGGCACCTTCC (F)
		TGACAATCTGGAAGCCACAG (R)
14	STIM2	GACGTCAGTATGCAGAACAG (F)
		GACCAACTGCTTCTCAGTTC (R)
15	ORAI1	ACGTGCACAATCTCAACTCG (F)
		AGAACTTGACCCAGCAGAGC (R)
16	ORAI2	ATGGTGGCCATGGTGGAGGT (F)
		TGCAGGCGCTGAAGGCAAT (R)
17	ORAI3	AAGCTCAAAGCTTCCAGCCGC (F)
		GGTGGGTACTCGTGGTCACTCT (R)
18	IP3R1	TGGACGAGGCTGGAAATGAA (F)
		CCTTCAGGCACAGAGACCAG (R)
19	IP3R2	ACCATCATCTCCACCCTCAT (F)
		AAGCAGACATGACAGTGAGAA (R)

(Continues)

TABLE 1 | (Continued)

Sl No	Gene	Sequence
20	IP3R3	AGCGATGCCTTATCATTGTAGA (F)
		CAAGTACGTCAAGAAGTGCCA (R)
21	PLA2G6	CTCAGCCTGACTCGAAAGAGCCTG (F)
		TGGGAGGGGAAGGTCGGTGAGTC (R)
22	B-Actin	TCAAGATCATTGCTCCTCCTGAG (F)
		ACATCGCTGGAAGGTGGACA (R)
23	GAPDH	TCACCAGGGCTGCTTTTAACTC (F)
		ATGACAAGCTTCCCGTTCTCAG (R)

(Figure 1H). The CRISPR-edited iPSCs with R747W mutation mirrored these phenotypes when compared with its isogenic control and validated our findings in the patient-derived iPSC cells with R741Q mutation (Figure S1A–H). Our observations are in line with previously published literature. A reduction in basal and maximal respiratory reserve was reported from different PD models with *Parkin* mutations (Stevens et al. 2015). Suppressed basal and maximal respiration along with decreased ATP production have been observed in iPSC-derived neurons with *SNCA* mutations (Zambon et al. 2019). Mitochondrial impairments were also observed in PD-neuronal precursor cells (Flierl et al. 2014). Overall, our results indicate that mitochondrial dysfunction can be an early indicator of disease in patients with PD-related mutations such as R741Q and R747W in *PLA2G6*.

3.2 | iPSCs with PD Mutations Exhibits a Compensatory Elevation in Glycolytic Activity

As described earlier, the patient-derived iPSCs and the CRISPR-edited mutant cells exhibited compromised mitochondrial respiration. A switch of energy metabolic pathways from OXPHOS to aerobic glycolysis (Warburg effect) is well characterized in various tumors and diseases as they have a higher energy demand (Chen et al. 2007). Glycolysis is a primitive metabolic pathway to extract energy from glucose. Each glucose molecule breaks down into pyruvate molecules through glycolysis. Glycolysis acts as the central ATP-producing pathway in most living cells. The pathway produces two molecules of ATP and NADH by oxidation by a series of coupled oxidations by enzymes without the involvement of molecular oxygen (Chaudhry and Varacallo 2024).

We used a Seahorse glycolytic stress assay to assess the glycolytic activity of these cells. The proton efflux rate was measured in a non-glucose-containing basal media-the catabolism of each molecule of glucose results in a net release of 2 H^+ ions. A serial injection of glucose, oligomycin, and 2-deoxyglucose (2-DG) was done to check various parameters related to the glycolytic activity. An enhanced glycolytic activity was detected in the patient-derived cells as compared to their familial control (Figure 2A). A significant elevation in glycolysis was observed in patient-derived iPSCs compared to control cells under basal conditions (Figure 2B). The addition of oligomycin inhibits mitochondrial ATP synthase, forcing glycolysis to work at its maximal capacity. A heightened glycolytic capacity and glycolytic reserve were seen in the patient-derived cells (Figure 2C,D) with respect to control cells but were not significant. The non-glycolytic acidification, the ECAR after the addition of 2-DG was significantly increased in the patient-derived cells (Figure 2E). Similarly, the mutant R747W iPSCs showed increased glycolytic activity and a similar increase in all the parameters (Figure S2A–E).

Recent studies suggest an elevated glycolytic profile in neurological disorders such as multiple sclerosis, amyotrophic lateral sclerosis, and Alzheimer's disease (Han et al. 2021; Tang 2020). A cell protective role of glycolysis in Alzheimer's disease by reducing β-amyloid aggregations was suggested (Newington et al. 2011). Further, *Parkin* deficiency was shown to increase glycolytic activity and decrease the reliance on mitochondria for energy. *Parkin* interacts with tumor suppressor genes p53 and PTEN; these are known to be involved in the metabolic reprogramming of cancer cells (Zhang et al. 2011). In contrast, an attenuation of PD progression by enhancement of glycolysis has been reported in animal models and clinical data (Cai et al. 2019). In keeping with these findings, our results suggest a compensatory elevation in glycolytic activity in iPSC cells with mutations in the *PLA2G6* gene that causes early-onset PD to circumvent the reduction in energy production by the impaired mitochondrial function.

3.3 | PLA2G6-R741Q iPSCs Show Reduced Mitochondrial Calcium Release

Mitochondria play a crucial role in maintaining cellular Ca^{2+} levels. Changes in mitochondrial ATP production are found to be closely linked to the variations in mitochondrial Ca^{2+} levels. Mitochondrial Ca^{2+} accumulation happens through the mitochondrial Ca^{2+} uniporter (MCU) in a respiration-dependent manner, and the Ca^{2+} is distributed close to the ER membranes (Gunter et al. 2000). High Ca^{2+} microdomains created by ER circumvent the lower affinity of MCU to Ca^{2+} ions. These Ca^{2+} microdomains are generated by the Ca^{2+} release from ER through inositol 1,4,5-trisphosphate receptors (IP_3Rs). These ER-released Ca^{2+} are transported across the outer mitochondrial membrane (OMM) by voltage-dependent anion channels (VDAC) and then from the intermembrane space to the mitochondrial matrix by MCU (Gunter et al. 2000; Surmeier et al. 2012).

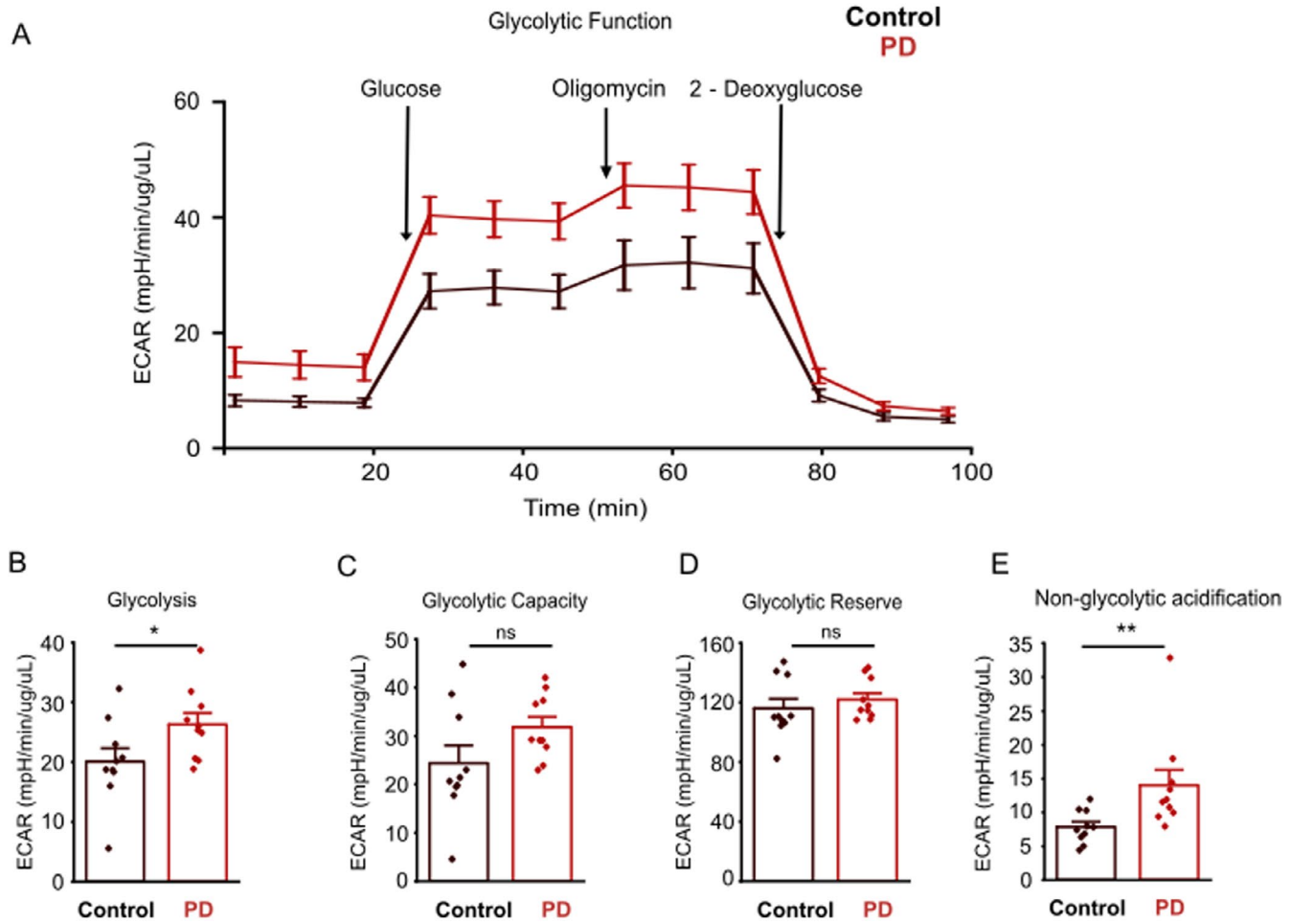

FIGURE 2 | PLA2G6-R741Q iPSCs exhibit an elevation in glycolytic activity. (A) Representative average trace of glycolytic function of PD iPSCs with R741Q-PLA2G6 (PD, red) and its control iPSCs (Control, black) from the Seahorse glycolytic stress assay (n=3 independent cell culture preparations, Control iPSC and PD iPSC–10 assay wells each), time of addition of glucose, oligomycin, and 2-deoxyglucose are marked with black arrows; (B) rate of glycolysis; (C) glycolytic capacity; (D) glycolytic reserve; (E) non-glycolytic acidification. (B–E) represented as mean ± SEM after normalization with protein content. Each dot represents a Seahorse assay plate well. The Shapiro–Wilk test was done to determine normality of the distribution; (B) the Mann–Whitney U test; (C–E) the Student's t-test with equal variance, $*p < 0.05$, $**p < 0.01$, ns-non-significant ($p \geq 0.05$). ECAR-extracellular acidification rate, Color codes: PD-patient-derived iPSCs with R741Q (Red), Control-familial control-derived iPSCs (Black).

Here, we looked at the mitochondrial Ca^{2+} release using the Rhod-2-AM dye (Figure 3A, individual cell responses of Control and PD iPSCs are shown in Figure S3B,C respectively). Similar to a recent study (Beccano-Kelly et al. 2023), we found the reduced release of Ca^{2+} from the mitochondria after depolarizing with FCCP, represented by Figure 3D. A concomitant increase in cytoplasmic Ca^{2+} was observed after the addition of FCCP, indicated by Fluo-4 AM (Figure S3D, individual cell responses of Control and PD iPSCs are shown in Figure S3E,F respectively). We also report significantly lower basal Ca^{2+} levels (Figure 3B) and higher variation in the PD iPSCs (Figure 3C) as compared to the control iPSCs. The change in fluorescence quantifies the reduced Ca^{2+} release (Figure 3E).

Ca^{2+} levels tightly regulate the expression of MCU. MCU activity is controlled by regulatory proteins, with which MCU makes the heteromeric protein complex. Mitochondrial Ca^{2+} uptake (MICU1, MICU2, and MICU3), MCU dominant negative beta subunit (MCUb), essential MCU regulator (EMRE), MCU regulator 1 (MCUR1), and SLC25A23 constitute the MCU heteromeric complex (Ludtmann and Abramov 2018). Expression patterns of these regulatory proteins are tissue-specific. An increase in protein levels of MCU and MICU1 expression in Hela cells with PD-linked LRRK2 mutations was reported (Matteucci et al. 2018). A recent study on mitochondrial Fe^{2+}–Ca^{2+} interaction showed a decrease in MCUB and NCLX in HEK cells with SNCA-A53T mutations after treatment with Fe^{2+} which promotes MCU complex assembly (Bharat et al. 2023). No change in expression levels of NCLX was observed in shPINK1 SHSY 5Y cells as compared to the control cells (Kostic et al. 2015). We analyzed the transcript levels of these genes to understand if the lower Ca^{2+} release from mitochondria can be explained by their expression levels in the iPSCs. However, the mRNA levels of *MCU* and accessory regulatory protein levels were not significantly altered between these genotypes (Figure 3F). In contrast, the mRNA levels of *MCUR1* and *MCUB* were found to be downregulated in the CRSIPR-engineered mutant line as

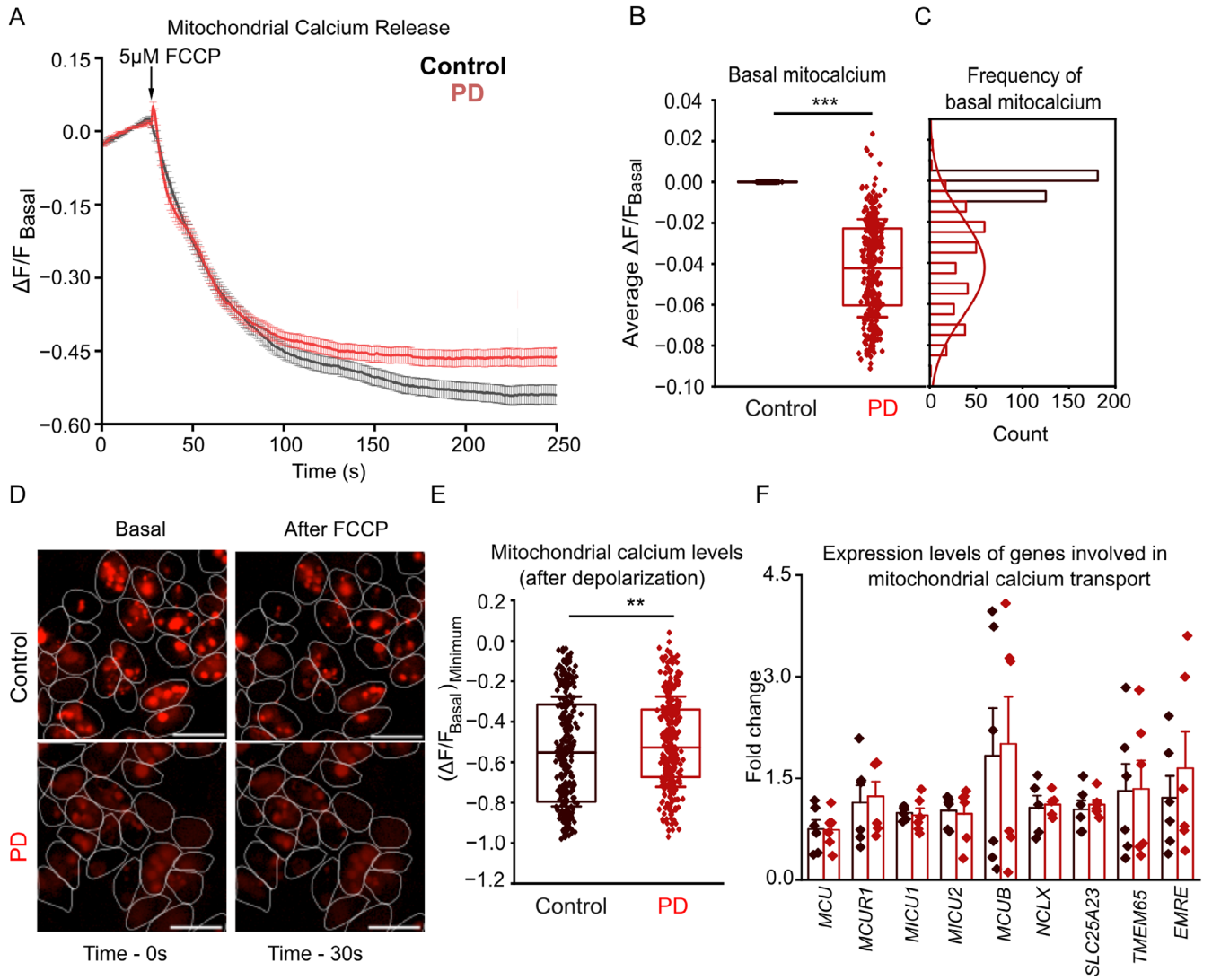

FIGURE 3 | PLA2G6-R741Q iPSCs show reduced mitochondrial calcium release. (A) Change in average traces of mitochondrial calcium release after treatment with 5 μM FCCP in Ca^{2+}-free HBSS in Control and PD iPSCs measured by Rhod-2 AM, a cell-permeant dye specific to mitochondrial calcium, represented as mean ± SEM at each measurement, n=3 (independent cell culture preparations), Control iPSC = 306 cells, PD iPSC = 323 cells; (B) average normalized Rhod-2 AM fluorescence of first 25 frames in the Ca^{2+}-free HBSS represented as the basal mitochondrial calcium (mitocalcium). Each dot represents an individual cell, and the 25th and 75th percentiles are represented as the box, the mean as the bar, and SEM as the error bars. ***$p < 0.001$, Mann-Whitney U test; (C) distribution of cells corresponding to different basal Rhod-2 AM fluorescence; (D) representative images of Control and PD iPSCs stained with Rhod-2 AM under the Airyscan microscope before and after the addition of FCCP, single Z plane, Scale bar-10 μm, cell peripheries marked with white lines; (E) change in mitochondrial calcium levels measured by the difference from basal to minimum fluorescence after the addition of FCCP. Each dot represents an individual cell, the 25th and 75th percentiles are represented as the box, the mean as the bar, the median as the dashed bar and SEM as the error bars. **$p < 0.01$, Mann-Whitney U test; (F) mRNA expression levels of genes involved in mitochondrial calcium transport were unaltered. n=6 (except *NCLX*, n=5) independent cell culture preparations, each dot represents a biological replicate. Mean ± SD, Student's t-test.

compared to the wild type (Figure S3A). The difference between the expression patterns could be due to a possible compensation mechanism that exists in the PD cell line with the R741Q mutation in the *PLA2G6* gene or because of the different genetic backgrounds.

Therefore, the reduced Ca^{2+} release could be due to lower levels of Ca^{2+} in the mitochondria. However, further experiments are required to understand what contributes to the lower mitochondrial Ca^{2+} levels and if the mutations in *PLA2G6* also affect the Ca^{2+} release and Ca^{2+} retention.

3.4 | PD Patient-Derived iPSCs Are More Prone to Changes in Mitochondrial Membrane Potential due to Uncoupling

As the mitochondrial function and Ca^{2+} release are affected in the PD cells, next we tested if the R741Q mutation changes the mitochondrial membrane potential ($\Delta\psi_m$). The $\Delta\psi_m$ is closely linked to the mitochondrial Ca^{2+} and the levels of ROS. Mitochondria utilize the electrochemical gradient potential created by the ETC to drive the ATP synthesis process. $\Delta\psi_m$ changes under dysregulated intracellular ionic homeostasis, ATP utilization, and functional

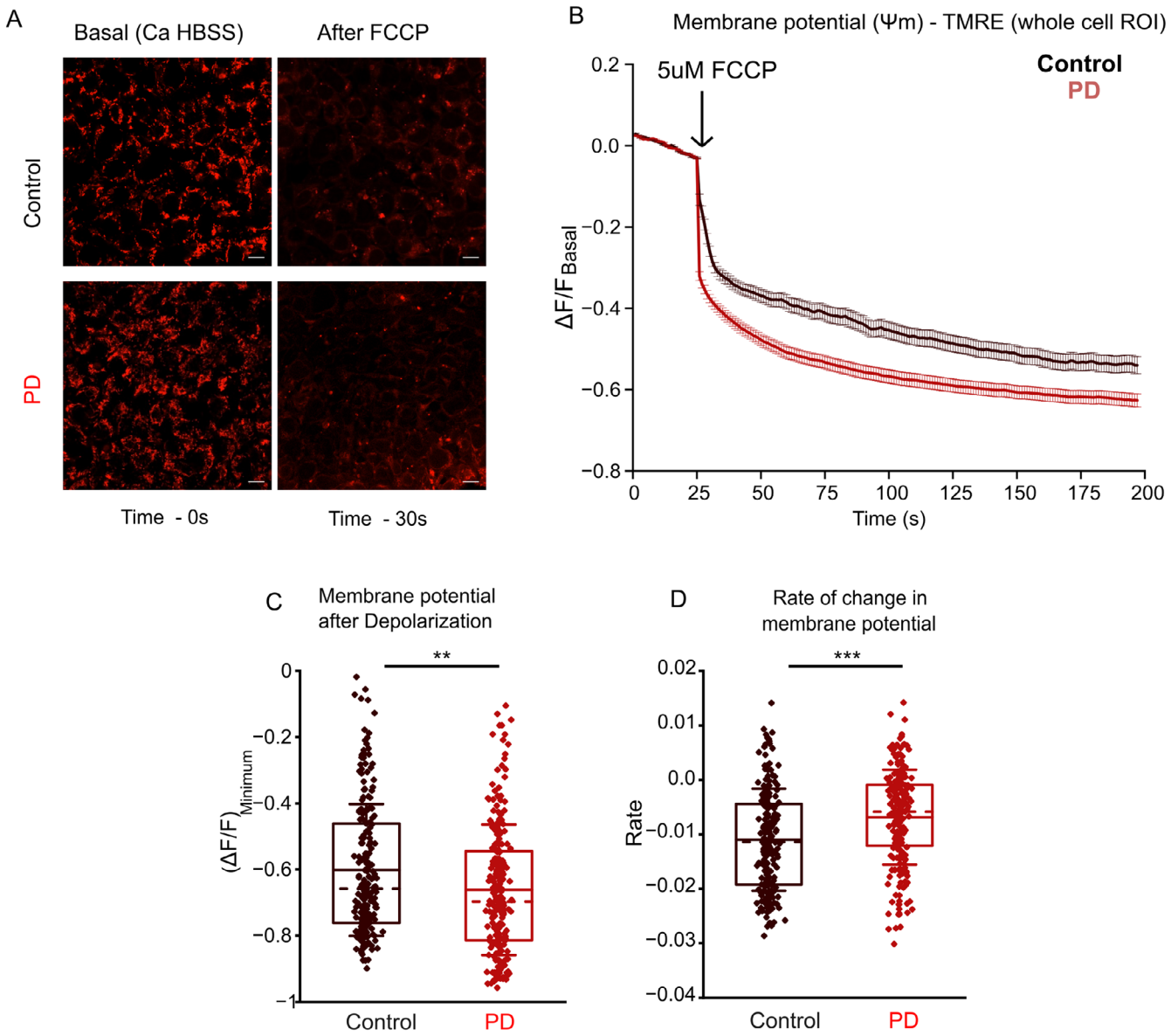

FIGURE 4 | PLA2G6-R741Q iPSCs are more sensitive to changes in mitochondrial membrane potential due to uncoupling. (A) Representative images of Control and PD iPSCs stained with TMRE-a mitochondrial membrane potential dye under the Airyscan microscope before and after the addition of FCCP, single Z plane, scale bar-10 μm; (B) change in average traces of mitochondrial membrane potential after uncoupling with 5 μM FCCP in HBSS in Control and PD iPSCs measured by TMRE, represented as mean ± SEM at each measurement, n=3 (independent cell culture preparations), Control iPSC = 213 cells, PD iPSC = 218 cells; and (C) change in mitochondrial membrane potential measured by the difference between the basal and the minimum fluorescence levels after the addition of FCCP. Each dot represents an individual cell, the 25th and 75th percentiles are represented as the box, the mean is the bar, the median is the dashed bar, and SEM is the error bar. $^{**}p < 0.01$, Mann-Whitney U test ; (D) the rate of change in mitochondrial membrane potential calculated by the average of the first derivative of the change in mitochondrial membrane potential from $t = 25$ to 50 s. Each dot represents an individual cell, and the 25th and 75th percentiles are represented as the box, the mean as the solid bar, the median as the dashed bar, and SEM as the error bars. $^{***}p < 0.001$, Mann-Whitney U test.

capacity of respiratory chains (Hu and Wang 2016; Perier and Vila 2012). Hence, these changes are interlinked, and looking at the $\Delta\psi_m$ could provide more insights into mitochondrial health. To this effect, we employed tetramethylrhodamine ethyl ester (TMRE) dye to assess the $\Delta\psi_m$ of PD and control iPSCs. After establishing the basal $\Delta\psi_m$ levels, we depolarized them using FCCP to see how they respond to the stress.

The PD iPSCs showed a drastic drop in the $\Delta\psi_m$ after the addition of FCCP (Figure 4A,B individual cell responses of Control and PD iPSCs are shown in Figure S4A,B respectively). PD mitochondria displayed significantly more depolarisation than the control mitochondria (Figure 4C). We also observed a significantly higher rate of depolarisation (calculated by the rate of reduction of fluorescence) in PD mitochondria upon the addition of FCCP (Figure 4D). To further demonstrate the extent of changes in the $\Delta\psi_m$ after the addition of FCCP, we calculated the raw fluorescent values into percentage difference from the basal fluorescence established (Figure S4C). The percentage decrease in $\Delta\psi_m$ upon the addition of FCCP was also found to be

significantly less in PD iPSCs as compared to the corresponding control iPSCs. Together, these results suggest that the PD mitochondria are more vulnerable to stressors like FCCP. It could also indicate that the PD iPSCs possess more unhealthy mitochondria than control iPSCs.

Remarkably, the changes we observed in $\Delta\psi_m$ are consistent with previous reports from other types of PDs. Specifically, flies lacking *iPLA2*-VIA (the *Drosophila* orthologue of *PLA2G6*) exhibited mitochondrial degeneration and decreased $\Delta\psi_m$ and ATP levels (Kinghorn et al. 2015). Similarly, PINK1 knockout mice exhibited a reduction in mitochondrial membrane potential, and overexpression of wild-type PINK1 restored hyperpolarized $\Delta\psi_m$ (Wang et al. 2011). In line with these studies, silencing of VPS13C is also associated with lower $\Delta\psi_m$ (Lesage et al. 2016). The PD-associated mutations in Fbxo7 also lead to reduced $\Delta\psi_m$ and increased ROS (Delgado-Camprubi et al. 2017). PINK1 is also known to be activated following $\Delta\psi_m$ depolarization (Jin et al. 2010; Kondapalli et al. 2012) and phosphorylates Parkin, together acting as a selective mitochondrial quality-control pathway (Narendra and Youle 2024). Interestingly, the PBMCs of PD patients also exhibit lower $\Delta\psi_m$ as compared to healthy controls (Qadri et al. 2018). This consistent reduction in mitochondrial membrane potential across model systems and forms of PD gives an early indication of the convergent mechanisms in mitochondrial dysfunction (Lesage et al. 2016; Wang et al. 2011).

3.5 | PD iPSCs Have Reduced SOCE

As described earlier, the mitochondria take up Ca^{2+} released by the ER through MCU and other channels. An impairment in store-operated Ca^{2+} release has been shown in patient *PLA2G6*-R747W fibroblasts and iPSC-derived DA neurons from PLA2G6 exon-2 knockout mice (Zhou et al. 2016). Hence, we hypothesized that the reduced mitochondrial Ca^{2+} could be an outcome of reduced stored Ca^{2+} levels or Ca^{2+} release. To address this, we used a previously established protocol using Fura-2 AM and Thapsigargin (TG) to assess intracellular Ca^{2+} levels.

The cell cytoplasm maintains a low Ca^{2+} level at the nanomolar scale. Cellular organelles such as ER, mitochondria, and lysosomes act as Ca^{2+} stores. The sarcoendoplasmic reticulum calcium ATPase (SERCA) pumps the extra Ca^{2+} from the cytoplasm to the ER to maintain the levels. TG irreversibly blocks SERCA and hence the ER Ca^{2+} uptake. In addition, the Ca^{2+} ions leak through various other channels located on the ER membrane (Lewis 2020; Parekh and Putney 2005; Prakriya and Lewis 2015; Putney et al. 2017). Therefore, after the addition of TG, we observe an increase in cytoplasmic Ca^{2+} levels, termed the store release (Parekh and Putney 2005). We observed impaired ER-related Ca^{2+} dynamics in R741Q iPSCs and R747W iPSCs compared to their respective controls (Figure 5A,B). We report a markedly reduced store release in R741Q iPSCs in comparison with the control iPSCs (Figure 5I), even though the basal levels of cytoplasmic Ca^{2+} were unaffected (Figure 5G). We compared the store release levels between the R747W iPSCs and WT iPSCs, and we found the same trend (Figure 5J). Similar to the patient-derived iPSCs, the basal Ca^{2+} was not significantly different in the R747W iPSCs with respect to its isogenic control (Figure 5H).

Further, we wanted to check the ER's Ca^{2+} intake upon adding back the physiological concentration of Ca^{2+} (2 mM). The cell perceives an empty ER as stress and triggers the SOCE. The stromal interaction molecule (STIM) located on the ER membrane senses the ER Ca^{2+} levels. It moves to the ER–Plasma membrane junction to recruit the Orai channels (Calcium release-activated channel protein) through which the Ca^{2+} enters the cytoplasm (Lewis 2020; Parekh and Putney 2005; Prakriya and Lewis 2015; Putney et al. 2017). Since we have blocked the SERCA, the Ca^{2+} levels increase in the cytoplasm. We noticed R741Q iPSCs uptake less Ca^{2+}, as described earlier (Figure 5C) (Zhou et al. 2016). Similarly, the R747W iPSCs also showed an impairment in the SOCE (Figure 5D).

We also found that Ca^{2+} entered at a sustainably lower rate in both cell lines with PLA2G6 mutations (Figure 5E,F). These results not only validate the previous reports linking *PLA2G6* with SOCE but also put forth a possible explanation of why mitochondria of PD iPSCs with *PLA2G6* mutations possess lower Ca^{2+} levels.

We detected no change in the protein levels of STIM1 (Figure S5A,B) or the mRNA levels of SOCE-related genes in the R741Q iPSCs (Figure S5E). Subsequently, we checked if we could rescue SOCE using a constitutive Orai activator (OA) along with Ca^{2+} addition after store release. 4-((5-phenyl-4-(trifluoromethyl) thiazol-2-yl) amino) benzoic acid (IA65) is identified as a constitutive Orai activator (OA) (Azimi et al. 2020). Both Control iPSCs and R741Q iPSCs showed an elevated uptake in Ca^{2+} in the presence of OA (Figure S5C,D). We used a higher concentration of 100 nM OA for our experiments. More experimentation with an OA titration needs to be performed to find an appropriate concentration at which the SOCE of PD iPSCs can be rescued to the levels of control iPSCs. The implications of these need to be further tested. Nonetheless, it validates our hypothesis that the impairment in SOCE is due to the changes at the regulatory levels and not because of changes in the expression of any SOCE-related genes. SOCE-dependent transcriptional regulation of dopaminergic neurons during development in *Drosophila* has been reported earlier (Pathak et al. 2015).

3.6 | Oxidative Stress and Autophagy in PD iPSCs

Finally, we checked the basal levels of ROS in the cells using DCFDA—an intracellular dye that fluoresces proportional to the level of ROS. Under healthy conditions, cells are equipped with a strong antioxidant system to maintain the ROS at optimal levels. The imbalance of ROS levels is referred to as oxidative stress, which is a characteristic of most neurodegenerative disorders, including PD. These higher ROS levels are even reported in non-disease-relevant cells in the early stages of PD (Zaltieri et al. 2015). We found that the basal ROS levels of PD iPSCs are consistently higher than the control iPSCs (Figure 6A,B), suggesting possible sequestering of unhealthy mitochondria. The ROS signals were quenched with 3 h of pre-treatment with 10 mm N-acetyl cysteine (NAC), an antioxidant (Figure S6A). The sulfane sulfur species derived from cysteine are likely the mediators of the acute antioxidative and cytoprotective effects of NAC observed in cell culture and animal experiments

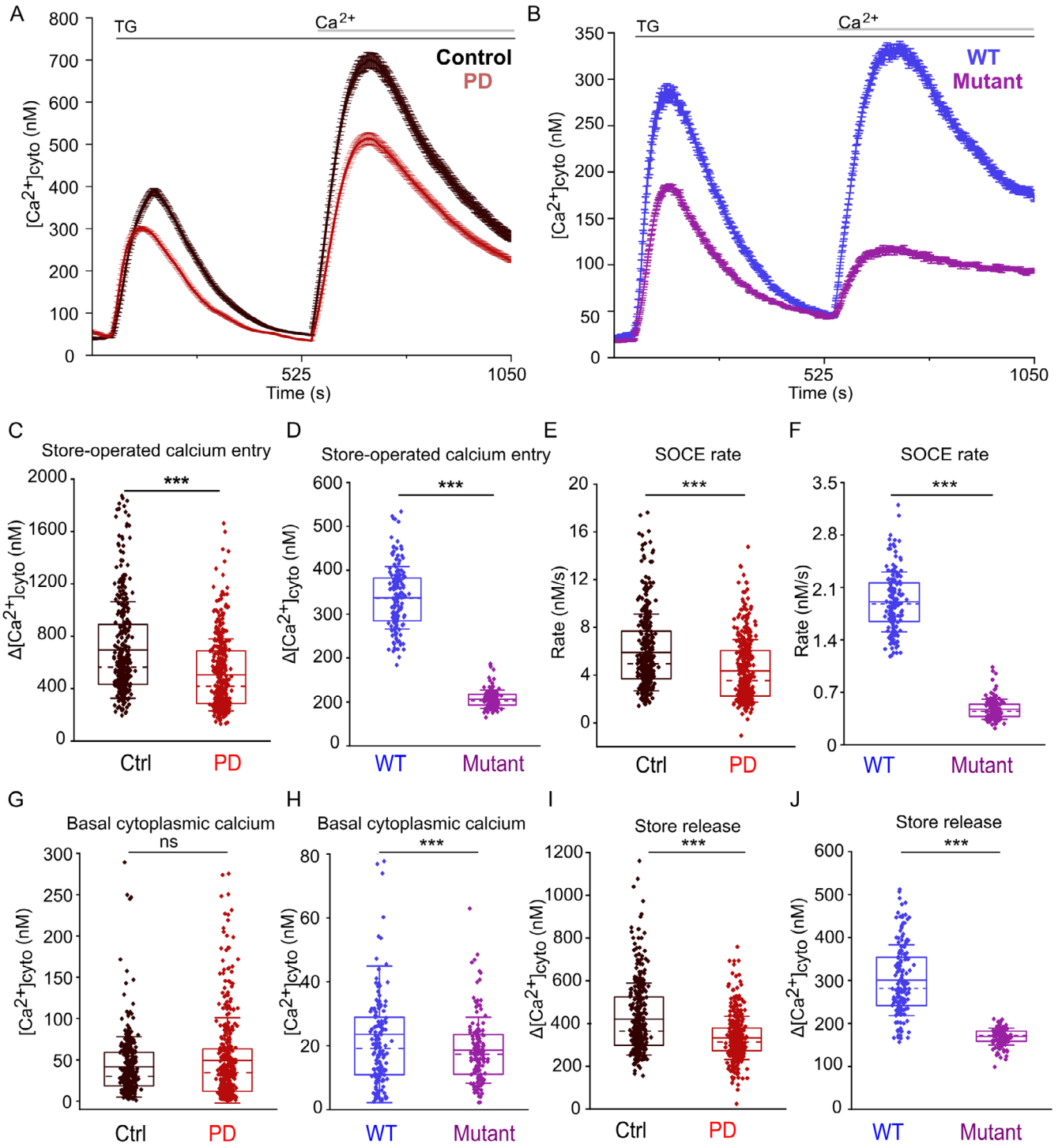

FIGURE 5 | PLA2G6-R741Q iPSCs have reduced store-operated calcium entry (SOCE). (A, B) Change in average traces of cytoplasmic calcium ($[Ca^{2+}]_{cyto}$) after blocking SERCA with 1 μM TG ($t = 50$ to 550 s) and adding 2 mM Ca^{2+} ($t = 550$ to 1050 s) in Ca^{2+} free HBSS in control (n = 4 independent cell culture preparations, 348 cells) and PD iPSCs (n = 5 independent cell culture preparations, 400 cells) (A) and WT (n = 3 independent cell culture preparations, 163 cells) and mutant iPSC (n = 4 independent cell culture preparations, 139 cells) (B) measured by Fura-2 AM, a ratiometric cell-permeant cytoplasmic calcium dye, represented as mean ± SEM at each measurement, n ≥ 4 together includes > 300 cells; (C, D) change in $[Ca^{2+}]_{cyto}$ after SOCE-Maximum change in $[Ca^{2+}]_{cyto}$ from the basal $[Ca^{2+}]_{cyto}$ after blocking SERCA with 1 μM TG and adding 2 mM Ca^{2+} in Ca^{2+} free HBSS; (E, F) the average rate of change in $[Ca^{2+}]_{cyto}$ due to SOCE calculated by the first derivative from $t = 550$ to 700 s in Ca^{2+} free HBSS; (G, H) basal $[Ca^{2+}]_{cyto}$ calculated by the average of $[Ca^{2+}]_{cyto}$ $t = 0$ to 50 s in Ca^{2+} free HBSS; (I, J) maximum change in $[Ca^{2+}]_{cyto}$ from the basal $[Ca^{2+}]_{cyto}$ after blocking SERCA with 1 μM TG ($t = 50$ to 550 s) in Ca^{2+} free HBSS. (C–J) each dot represents an individual cell, and the 25th and 75th percentiles are represented as the box, the mean as the solid bar, the median as the dashed bar and SEM as the error bars. ***$p < 0.001$, ns-non-significant ($p \geq 0.05$), Mann- Whitney U test. PD-Patient-derived iPSCs with R741Q-PLA2G6 (Red), Control-familial control-derived iPSCs (Black), Mutant-CRISPR-engineered iPSCs with R747W- PLA2G6 (Purple), WT-Wild type iPSCs (Blue).

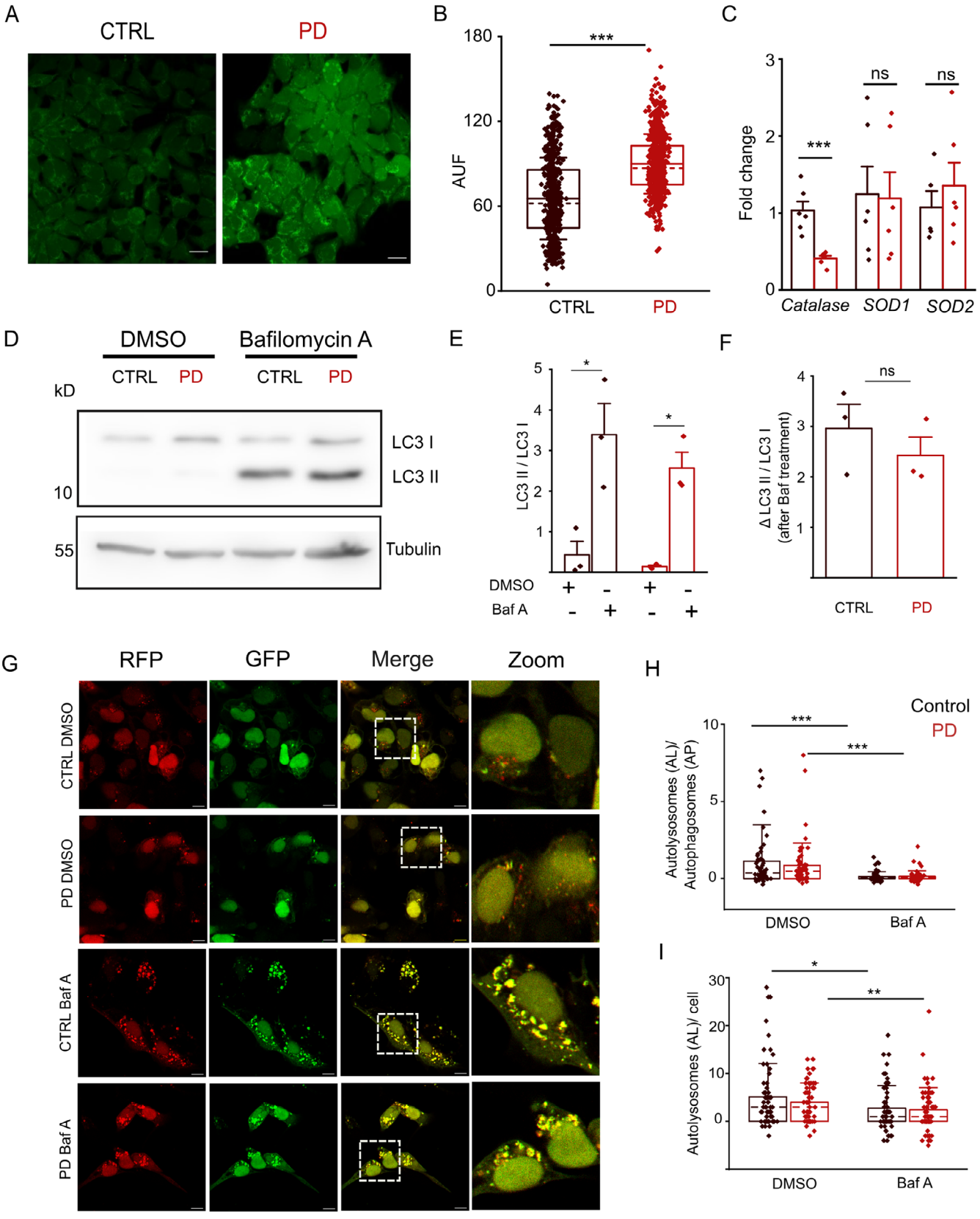

FIGURE 6 | Legend on next page.

(Ezeriņa et al. 2018; Pedre et al. 2021). A previous study with fibroblasts from *PLA2G6* ANAD and INAD patients has shown phenotype corrections after treating with Vitamin E, another category of antioxidants (Villalón-García et al. 2022).

The antioxidant system of cells largely comprises enzymes—Catalase, superoxide dismutase 1 and 2 (SOD1, SOD2), glutathione-glutaredoxin (Grx) system, and thioredoxin. We observed a significant reduction in the mRNA levels of *catalase*

FIGURE 6 | PLA2G6-R741Q iPSCs show higher oxidative stress but unaltered autophagic flux. (A) Confocal images of Control and PD iPSCs stained with DCFDA, a ROS-specific dye at the basal level, Z- Stack projection, Scale bar- 20 μM; (B) basal ROS calculated using fluorescence from the frame with maximal Z-projection. Each dot represents an individual cell, and the 25th and 75th percentiles are represented as the box, the mean as the solid bar, the median as the dashed bar, and SEM as the error bars. ***$p < 0.001$, Mann-Whitney U test. n = 5 independent cell culture preparations, Control iPSC = 536 cells and PD iPSC = 687 cells; (C) mRNA levels of *Catalase* and other antioxidant enzymes. n = 6 independent cell culture preparations, each dot represents a biological replicate. Mean ± SD. Student' *t*–test ***$p < 0.001$; (D) representative images of the western blot of protein lysates of PD and iPSCs treated with DMSO (vehicle) or bafilomycin A probed for LC3 II, LC3 I, and housekeeping protein β- Tubulin; (E) LC3 II/LC I ratio of each group: Control iPSC (black) and PD iPSC (red) with DMSO or bafilomycin A. Each dot represents a biological sample, n = 3 independent cell culture preparations, paired *t*-test, *$p < 0.05$, SEM ± SD; (F) autophagic flux after treatment with bafilomycin A, calculated as the increase in LC3 II/LC3 I from the basal levels, each dot represents a biological sample, n = 3 independent cell culture preparations, paired *t*-test, ns- non-significant. SEM ± SD; (G) Representative images of CTRL iPSCs and PD iPSCs treated with DMSO (vehicle) or bafilomycin A from the tandem fluorescent quenching assay (TFQA). Left to Right: Panel 1-representative images under the red channel (RFP), Panel 2-corresponding images under the green channel (GFP), Panel 3-merge of both channels and Panel 4-zoomed images of the cells (Scale bar-10 μM). Different treatment groups are labeled;. (H) ratio of autolysosomes (AL) to autophagosomes (AP); (I) Quantification of the number of autolysosomes per cell. (H,I) Each dot represents an individual cell, the median as the dashed bar, and SEM as the error bars. *$p < 0.05$, **$p < 0.01$, ***$p < 0.001$, ns-non-significant ($p \geq 0.05$), Shapiro-Wilk test, Mann- Whitney U test. PD-patient-derived iPSCs with R741Q-PLA2G6 (Red), Control-familial control-derived iPSCs (Black).

from the PD iPSCs (Figure 6C), indicating a dysregulated ROS scavenging system. Previous unpublished results from the lab had a direct implication for decreased catalase expression and activity in *Drosophila* PD models, which prompted us to look at this in our cell culture experiments. We validated the reduction in catalase mRNA expression in our CRISPR-engineered cell lines and found a substantial reduction in the mutant cell line (R747W) (Figure S6B), suggesting the changes in catalase are possibly a direct consequence of PD-associated *PLA2G6* mutations. This explains, at least in part, the higher ROS levels observed in the PD iPSCs compared to the controls. ROS-induced PD pathology has been demonstrated in various models with *Parkin*/*PINK1*, *DJ-1*, and *LRRK2* mutations (Angeles et al. 2011; Joselin et al. 2012; Xiao et al. 2017). As we were successful at reducing the ROS levels using NAC treatment, we decided to check if NAC treatment can also rescue the catalase mRNA levels. Even though we observed a slight improvement in catalase expression levels after 3 h of NAC treatment, they were not statistically significant (Figure S6C). This is not surprising as a direct effect of NAC on catalase is unknown, as opposed to its strong link to the glutathione system.

Autophagic clearances of toxic materials and unhealthy organelles work as an additional mechanism to ensure the cell's homeostatic balance before signaling cell death. Autophagic mechanisms are broadly categorized into macro and micro autophagy. Mitophagy, a specialized macro autophagy that recycles and removes unhealthy mitochondria from the cytoplasm, helps in adequate aerobic respiration and reduces ROS levels (Wei et al. 2015; Xiao et al. 2022; Youle and Narendra 2011; Zorov et al. 2014). ROS triggers both non-selective autophagy and mitophagy in a dose-dependent manner, resulting in cell death (Frank et al. 2012). Conversely, neuroprotective effects of mitophagy have also been documented (Koentjoro et al. 2017). However, prolonged dysregulation in autophagy or mitophagy and increased ROS production are strongly indicative of neuronal cell death in PD models (Trist et al. 2019; Xiao et al. 2022). Impaired autophagy, in particular, elevated levels of mitophagy, are described as a hallmark of cells harboring PD mutations (Koentjoro et al. 2017; Lesage et al. 2016; Xiao et al. 2017, 2022). We looked at the autophagic marker, Microtubule-associated protein 1A/1B-light chain 3 (LC3), to assess the autophagy levels in our iPSC cultures. LC3 is a ubiquitously expressed soluble protein with two different forms. LC3 I is localized in the cytoplasm and, upon lipidation, forms the LC3 II. A phosphatidylethanolamine side chain gets conjugated to the LC3 I during the lipidation process and is recruited into the autophagic membranes (Tanida et al. 2002, 2004). The LC3 II gets degraded when the autophagosomes fuse with lysosomes. Hence, monitoring the changes in the presence of LC3 II and the ratio of LC3 II to LC3 I helps in assessing the alterations in autophagy (Ganley et al. 2011; Yamamoto-Imoto et al. 2022).

Since autophagy is one of the basal cell regulatory mechanisms, the turnover rate is very high. Previous studies have described that treating with inhibitors such as Bafilomycin A (Baf A) enables better quantitation of autophagic turnover. Baf A is a vascular H^+—ATPase; therefore, it blocks the LC3 II degradation (Mizushima and Yoshimori 2007; Yoshimori et al. 1991). As it is a late-autophagic inhibitor, no further LC3 lipidation happens. Hence, it allows for a robust assessment of autophagic flux. Defective autophagy has been documented in PD brains (Alvarez-Erviti et al. 2010; Anglade et al. 1997). Dysfunctional autophagy in the fibroblasts of PLA2G6 knockout mice was reported earlier, and this could be rescued by overexpressing the *PLA2G6* gene (Zhou et al. 2016). We could not detect a significant change in autophagic flux of the PD iPSCs in the presence of Baf A with respect to that of control iPSCs (Figure 6D–F). The blots used for quantification of the flux and total LC3 II are shown in Figure S6D. There was a trend of decreased flux in the PD samples, but this was not a strong phenotype contrary to what is reported in neuronal cultures of PD. To confirm these findings in single cells, we used the RFP-GFP tandem fluorescence plasmid to overexpress LC3 in the patient-and control iPSCs. The GFP is quenched in the acidic pH of lysosomes, and the red puncta are the autolysosomes, whereas the yellow signals are indicative of autophagosomes (Figure 6G). The data followed the same trend as the immunoblotting results. Significant differences were seen only in the Baf A treated cells and vehicle control within the same group for autolysosomes to autophagosomes ratio (Figure 6H) and total autolysosomes per cell (Figure 6I). The autophagosomes per cell and total LC3 puncta were also

not significantly different between the control and PD groups (Figure S6E,F). This is not surprising, as autophagic flux and related parameters could be a tissue or cell-specific trait more prominent in high-energy demanding cells like the DA neurons in the context of PD.

4 | Discussion

Understanding cellular and molecular changes during disease progression in a systematic manner is crucial for early detection and symptom management. Here, we demonstrate that cellular phenotypes such as mitochondrial dysfunction and associated Ca^{2+} dyshomeostasis due to SNPs in *PLA2G6* are manifested even in undifferentiated stem cells. In similar lines, a study utilizing sporadic PD fibroblasts and iPSC-DA neurons from the same patient showed specific changes in ROS, mitochondrial function, and autophagy in both cell types. The findings clearly indicated that basic PD processes are convergent in the peripheral and neuronal phenotypes (Corenblum et al. 2023). A study examining the interaction between PINK1 and LRRK2 found the expression of the latter deregulated not only in the neurons but also in the fibroblasts of PINK1-PD patients (Azkona et al. 2018). Higher vulnerability to rotenone-induced cell death was shown in sporadic PD fibroblasts, but changes in autophagy could not be detected (Ambrosi et al. 2014). Mitochondrial phenotypes are well documented in fibroblasts harboring *LRRK2*, *PINK1*, and *Parkin* mutations (Caesar et al. 2015; Grünewald et al. 2010; Rakovic et al. 2010; Smith et al. 2016; van der Merwe et al. 2014; Yakhine-Diop et al. 2014). Therefore, these peripheral tissues and iPSC lines from PD patients provide an attractive model to study the early disease-specific changes in addition to serving as biomarker and drug testing platforms. To our knowledge, this is the first study to look at non-neural PLA2G6 PD phenotypes and show convergence to the key pathways reported in recessive parkinsonism.

The effects of mitochondrial and intracellular Ca^{2+} imbalance on PD are inconclusive, possibly because these changes are specific to the disease-causing mutations (Beccano-Kelly et al. 2023; Dey et al. 2020; Gandhi et al. 2009; Ludtmann and Abramov 2018; Scorziello et al. 2020; Zampese and Surmeier 2020). The causal-effect relations between changes in different mitochondrial parameters remain unclear. Nonetheless, the accumulation of unhealthy mitochondria and its inability to meet the cellular energy requirements seem to be one of the earliest detectable phenotypes of PD. Furthermore, based on our work, mitochondrial dysfunction may happen early on during the disease onset, and published literature indicates that this happens independently of the unfolded protein aggregation (Risiglione et al. 2021; Zaltieri et al. 2015; Zampese and Surmeier 2020).

The decreased mitochondrial capacity indicated by reduced basal respiration, maximal respiration, and ATP production of PD iPSCs suggests that these cells have defective oxidative energy metabolism. The reduced mitochondrial respiration dependent on complex I and II and reduced coupling efficiency were earlier reported from the *PLA2G6* KO *Drosophila* model. It was correlated with elevated lipid peroxidation and reduced mitochondrial membrane potential and validated in human fibroblasts with R747W mutation in *PLA2G6* (Kinghorn et al. 2015). Along the same lines, the ATP levels were demonstrated to be less in SHSY-5Y-derived dopaminergic neurons transfected with R741Q *PLA2G6* construct after being treated with rotenone (Chiu et al. 2017). In addition, a recent structural analysis of PLA2G6 protein has shown an interaction between ATP and the Ankyrin domain of PLA2G6 (Malley et al. 2018). However, it is uncertain if this interaction has any influence on the mitochondrial phenotypes we observe. The DA neurons in the SNpc, the primary affected cell type in PD, possess a higher energy requirement due to their pace-making activity and long axon projection with thin or no myelination (Duda et al. 2016; Grace and Onn 1989; Pissadaki and Bolam 2013). Previous studies have suggested that the mitochondrial defects that we demonstrate in iPSCs become more prominent over the course of neuronal differentiation (Liang et al. 2020). Hence, it is reasonable to propose that these phenotypes will be more pronounced in NSCs and neurons. Cells rely on pyruvate levels to maintain the SRC and increase glycolytic activity under high energy demand (Marchetti et al. 2020). Along with compensating for the reduction in ATP production by the PD mitochondria, this could be a possible explanation for the concomitant increase in the glycolytic level and glycolytic capacity in the iPSCs harboring *PLA2G6* mutations (Cai et al. 2019; Yadava and Nicholls 2007).

A switch from mitochondrial metabolism to glycolytic signature is known to occur during the dedifferentiation of somatic cells and reprogramming to iPSCs. This transition to glycolysis helps meet the anabolic requirements for both dedifferentiation and proliferation (Folmes et al. 2011; Panopoulos et al. 2012). The reprogramming trajectory also involves huge changes in the epigenetic landscape. While it is known that iPSCs retain an epigenetic memory of their tissue of origin (Kim et al. 2010), extended passaging is thought to erase it to a large extent (Polo et al. 2010). We have not used early passage iPSCs in our experiments and believe that the alteration in the metabolic status of the control and PD iPSCs is indicative of cellular pathology rather than this being an artefact of the reprogramming process. These changes are also mirrored by the CRISPR-edited R747W cells where the background and reprogramming techniques are entirely different. In PD patient peripheral blood mononuclear cells, mitochondrial dysfunction and increased glycolysis were seen in early and prodromal stages (Smith et al. 2018), confirming that cellular pathology changes can be detected in non-neural cells.

PD with *PINK1* deficiency has been linked to an overload of mitochondrial Ca^{2+} and the opening of mPTP. α-Synuclein has been found to form plasma membrane pores, thereby allowing extracellular Ca^{2+} to enter the cytoplasm and result in elevated cytoplasmic Ca^{2+} levels. It increases the demand for ATP to restore the cytoplasmic Ca^{2+} levels, adding more burden to the already impaired mitochondria. It is also shown that intracellular Ca^{2+} has a positive impact on α- Synuclein aggregation, making a vicious cycle and increasing PD pathology (Gandhi et al. 2009). In contrast, a mouse model of INAD, another PLA2G6-associated neurodegenerative disorder, has demonstrated a significant reduction in mitochondrial Ca^{2+} uptake and retention in the mice hypomorph in the *PLA2G6* gene. They further proposed that the reduced mitochondrial Ca^{2+} capacity could lead to increased

cellular vulnerability to mitochondrial Ca^{2+} overload (Strokin and Reiser 2016). Taken together, dysregulated mitochondrial Ca^{2+} homeostasis has been linked to various forms of PD (Dey et al. 2020; Ludtmann and Abramov 2018; Surmeier et al. 2012). Our PD iPSCs showed a reduction in basal mitochondrial Ca^{2+} level and also Ca^{2+} release upon depolarization. A slightly reduced level of mitochondrial Ca^{2+} in iPSC-derived DA neurons with GBA-L444P mutation along with an altered PLA2G6 level has been reported recently (Beccano-Kelly et al. 2023).

Further, $\Delta\psi_m$ creates the chemical gradient to facilitate the Ca^{2+} sequestration and regulate the ROS production. Hence, the change in mitochondrial Ca^{2+} could be either due to the change in $\Delta\psi_m$ or due to the impaired SOCE, which is the main source of the mitochondrial Ca^{2+} (Chiu et al. 2017; Ke et al. 2020; Kinghorn et al. 2015; Marchetti et al. 2020; Scorziello et al. 2020; Zampese and Surmeier 2020). The attenuated $\Delta\psi_m$ can alter the MCU activity. It is important to note that we observed no difference in the mRNA levels of any of the MCU-complex-associated genes in the patient-derived PD iPSCs. Besides, the $\Delta\psi_m$ changes under dysregulated intracellular ionic homeostasis, ATP utilization, and capacity of respiratory chains. Hence, it is interesting how, irrespective of the consistent trends in alterations in ERC, $\Delta\psi_{m,}$ and ROS levels, the mitochondrial Ca^{2+} shows a change in the opposite direction. We also need to take into consideration that depolarized mitochondria can activate the *PLA2G6* gene and lead to increased release of free fatty acids and change in mPTP (Broekemeier et al. 2002). It is known that the change in PLA2G6 levels and structure causes ER stress, but the mechanism by which it happens is unclear. Ke et al. reported that treatment with azoramide, a chemical used for hypertension, can rescue SOCE-associated Ca^{2+} homeostasis and changes in mitochondrial parameters in the iPSC-derived dopaminergic neurons with *PLA2G6* D331Y mutation (Ke et al. 2020). PLA2G6 is localized in the cytosol and membranes of ER, mitochondria, and lysosomes. It was earlier reported that the levels of the PLA2G6 (L) variant, which localizes in the plasma membrane, were reduced in fibroblasts with R747W *PLA2G6* (Zhou et al. 2016). It is crucial to note that our primer sequences were not designed to identify expression levels in a splice specific manner. It is essential to understand if the localization pattern of PLA2G6 can directly induce these defects and also how these mutations lead to PM-ER-mitochondria interactions.

We observed an elevated ROS level in our PD iPSCs and an accompanying decrease in the catalase mRNA expression. There is no known direct interaction between the PLA2G6 and catalase. Additional experiments and bioinformatic analyses are required to elucidate how the SNPs in PLA2G6 lead to decreased expression of catalase through direct or indirect pathways. The increase in mitochondrial stress and ROS levels and a concomitant decrease in $\Delta\psi_m$ are consistently observed from various in vitro and in vivo models of familial and sporadic PD from late pathological states in dopaminergic neurons and non-neuronal brain cells (Beccano-Kelly et al. 2023; Bharat et al. 2023; Dey et al. 2020; Henrich et al. 2023; Imaizumi et al. 2012; Ke et al. 2020; Palacino et al. 2004; Scorziello et al. 2020; Surmeier et al. 2012; Zanellati et al. 2015). Our earlier study on *STIM1* KD NPCs (GEO Series accession number GSE109111) with reduced SOCE showed a significant reduction in the thioredoxin and thioredoxin reductase 1 enzymes (data not shown, Gopurappilly et al. 2018). Together, these indicate a faulty or suboptimal antioxidant system that may lead to higher ROS levels.

Autophagic defects are observed in different PLAN disorders, including PD (Arber et al. 2016; Kinghorn and Castillo-Quan 2016; Liu et al. 2024; Zhou et al. 2016). Autophagic dysfunction in the *PLA2G6* PD from patient fibroblasts with R747W mutation and SHSY-5Y dopaminergic neurons with R741Q mutation in *PLA2G6* is reported (Chiu et al. 2017; Zhou et al. 2016). In addition, loss of function PLA2G6 mutation in the *Drosophila* model demonstrated suboptimal retromer function by destabilizing its subunits Vps26 and Vps35 (Lin et al. 2018). Lysophospholipids and free fatty acids generated by the catalytic activity of PLA2G6 can increase the fluid mobility and non-bilayer structures in its immediate environment and can cause increased membrane fusion (Arber et al. 2016; Balsinde and Balboa 2005). This could be a plausible explanation for the increased autophagy in NBIA and INAD (PLAN disorders with deficient PLA2G6 catalytic activity). *PLA2G6*-PD in India is frequently caused by the mutation PLA2G6:c.2222G>A (p.Arg741Gln, R741Q) and is not associated with brain iron accumulation (Magrinelli et al. 2022). The loss of catalytic activity of PLA2G6 is strongly associated with NBIA and INAD, but not with PD-associated mutations (Engel et al. 2010). The loss of such activity is suggested to be the cause of abnormalities in lipid homeostasis leading to the accumulation of abnormal lipid membranes. Though lipid peroxidation has been reported in some studies with c.2239C>T (R747W) mutations in fibroblasts of non-Asian origin (Kinghorn et al. 2015; Sun et al. 2021), its role in PD-related *PLA2G6* mutations remains inconclusive. This published information along with our use of reprogrammed iPSCs in contrast to primary cells deterred us from evaluating the status of lipid peroxidation/lipofuscin deposition in the patient iPSCs. At the iPSC level, we could not see a significant change in the autophagic flux in the PD cells after treatment with the inhibitor Bafilomycin A. Autophagic dysfunction in the context of genetic PD with mutations in *SNCA*, *LRRK2*, *PINK1*, *Parkin*, *GBA* genes and some others is well documented and reviewed in detail (Hou et al. 2020; Nechushtai et al. 2023). The cell type explored in the available literature has almost always been the dopaminergic (DA) neuron. The autophagic dysfunction in DA neurons is directly linked to its high energy demand and increased vulnerability owing to the production and release of dopamine. The divergence from these published reports in our case could be the use of a different model system that does not reflect the interconnected network of α-synuclein, dopamine, and neuron-specific protein aggregation pathways. Together, an impaired autophagic function may lead to PD pathogenesis; however, these effects are dependent on the mutation and cell type being investigated.

This work demonstrates the potential of iPSCs and iPSC-derived cells in characterizing PD associated with SNPs in the *PLA2G6* gene. With parallel phenotypes in CRISPR-engineered iPSCs, we have successfully established that these changes are unambiguously due to the *PLA2G6* mutations. It is pivotal to appreciate that these changes are even evident in undifferentiated cells. Moreover, our study substantiates the use of iPSCs as a lead-in model to validate the efficacy of PD drugs in screening and toxicity studies. Regardless, it is crucial to look at how these changes progress over differentiation and connect them

to observable clinical phenotypes such as loss of motor coordination. Due to the extremely rare nature of the disease, we did not have multiple iPSC lines to confirm our findings. Even though the CRISPR-engineered iPSCs validate the results, it would be more beneficial to use patient iPSCs with PD-specific *PLA2G6* mutations to avoid any biases. Interactome, differential gene expression, and localization studies need to be done to understand the chronology of manifestation or the cause-consequence segregation of the observed defects. Importantly, we have limited the study to an early cell state, i.e., iPSCs, and the findings need to be replicated in midbrain neural precursors and neurons for direct correlation with the progression of disease pathology.

Author Contributions

Thasneem Musthafa: conceptualization, data curation, writing – original draft, methodology, formal analysis, investigation, visualization. **Syed Kavish Nizami:** methodology, visualization. **Ankita Mishra:** resources, methodology. **Gaiti Hasan:** writing – review and editing, supervision, resources, software, validation, visualization. **Renjitha Gopurappilly:** conceptualization, funding acquisition, writing – review and editing, supervision, project administration, validation, visualization.

Acknowledgments

This work was supported by the DBT/Wellcome Trust India Alliance Early Career Fellowship [IA/E/18/1/504319] awarded to R.G. We thank the Central Imaging and Flow Cytometry facility (CIFF), Stem Cell Culture Facility, and Biosafety level-2 laboratory facility at the National Centre for Biological Sciences, Bangalore, India. The authors thank Dr. Biju Viswanath, National Institute of Mental Health and Neurosciences, Bangalore, India, for the patient and control PD blood samples for iPSC derivation. We acknowledge Pragnya Chakraborty, National Centre for Biological Sciences, for the help with Calcium Imaging, and Preeti Jindal, NKure Therapeutics Pvt. Ltd., for the help with LC3 puncta quantification.

Conflicts of Interest

The authors declare no conflicts of interest.

Data Availability Statement

All the primary (raw) and secondary data used in the paper can be made accessible on request. Please write to the corresponding authors for the same. The same will be submitted to the Research Integrity Office, NCBS-TIFR Bangalore.

References

Alvarez-Erviti, L., M. C. Rodriguez-Oroz, J. M. Cooper, et al. 2010. "Chaperone-Mediated Autophagy Markers in Parkinson Disease Brains." *Archives of Neurology* 67, no. 12: 1464–1472. https://doi.org/10.1001/archneurol.2010.198.

Ambrosi, G., C. Ghezzi, S. Sepe, et al. 2014. "Bioenergetic and Proteolytic Defects in Fibroblasts From Patients With Sporadic Parkinson's Disease." *Biochimica et Biophysica Acta (BBA) – Molecular Basis of Disease* 1842, no. 9: 1385–1394. https://doi.org/10.1016/j.bbadis.2014.05.008.

Angeles, D. C., B.-H. Gan, L. Onstead, et al. 2011. "Mutations in LRRK2 Increase Phosphorylation of Peroxiredoxin 3 Exacerbating Oxidative Stress-Induced Neuronal Death." *Human Mutation* 32, no. 12: 1390–1397. https://doi.org/10.1002/humu.21582.

Anglade, P., S. Vyas, F. Javoy-Agid, et al. 1997. "Histology and Histopathology From Cell Biology to Tissue Engineering Apoptosis and Autophagy in Nigral Neurons of Patients With Parkinson's Disease." *Histology and Histopathology* 12: 25–31. https://doi.org/10.14670/HH-12.25.

Arber, C. E., A. Li, H. Houlden, and S. Wray. 2016. "Review: Insights Into Molecular Mechanisms of Disease in Neurodegeneration With Brain Iron Accumulation: Unifying Theories." *Neuropathology and Applied Neurobiology* 42, no. 3: 220–241. https://doi.org/10.1111/nan.12242.

Azimi, I., R. J. Stevenson, X. Zhang, et al. 2020. "A New Selective Pharmacological Enhancer of the Orai1 Ca2+ Channel Reveals Roles for Orai1 in Smooth and Skeletal Muscle Functions." *ACS Pharmacology & Translational Science* 3, no. 1: 135–147. https://doi.org/10.1021/acsptsci.9b00081.

Azkona, G., R. López de Maturana, P. del Rio, et al. 2018. "LRRK2 Expression Is Deregulated in Fibroblasts and Neurons From Parkinson Patients With Mutations in PINK1." *Molecular Neurobiology* 55, no. 1: 506–516. https://doi.org/10.1007/s12035-016-0303-7.

Balsinde, J., and M. Balboa. 2005. "Cellular Regulation and Proposed Biological Functions of Group via Calcium-Independent Phospholipase A in Activated Cells." *Cellular Signalling* 17, no. 9: 1052–1062. https://doi.org/10.1016/j.cellsig.2005.03.002.

Beccano-Kelly, D. A., M. Cherubini, Y. Mousba, et al. 2023. "Calcium Dysregulation Combined With Mitochondrial Failure and Electrophysiological Maturity Converge in Parkinson's iPSC-Dopamine Neurons." *iScience* 26, no. 7: 107044. https://doi.org/10.1016/j.isci.2023.107044.

Bharat, V., A. S. Durairaj, R. Vanhauwaert, et al. 2023. "A Mitochondrial Inside-Out Iron-Calcium Signal Reveals Drug Targets for Parkinson's Disease." *Cell Reports* 42, no. 12: 113544. https://doi.org/10.1016/j.celrep.2023.113544.

Broekemeier, K. M., J. R. Iben, E. G. LeVan, E. D. Crouser, and D. R. Pfeiffer. 2002. "Pore Formation and Uncoupling Initiate a Ca^{2+} -Independent Degradation of Mitochondrial Phospholipids." *Biochemistry* 41, no. 24: 7771–7780. https://doi.org/10.1021/bi020157z.

Caesar, M., S. Felk, J. O. Aasly, and F. Gillardon. 2015. "Changes in Actin Dynamics and F-Actin Structure Both in Synaptoneurosomes of LRRK2(R1441G) Mutant Mice and in Primary Human Fibroblasts of LRRK2(G2019S) Mutation Carriers." *Neuroscience* 284: 311–324. https://doi.org/10.1016/j.neuroscience.2014.09.070.

Cai, R., Y. Zhang, J. E. Simmering, et al. 2019. "Enhancing Glycolysis Attenuates Parkinson's Disease Progression in Models and Clinical Databases." *Journal of Clinical Investigation* 129, no. 10: 4539–4549. https://doi.org/10.1172/JCI129987.

Chaudhry, R., and M. Varacallo. 2024. "*Biochemistry, Glycolysis*." In: StatPearls [Internet]. Treasure Island (FL): StatPearls Publishing. https://www.ncbi.nlm.nih.gov/books/NBK482303/.

Chen, Z., W. Lu, C. Garcia-Prieto, and P. Huang. 2007. "The Warburg Effect and Its Cancer Therapeutic Implications." *Journal of Bioenergetics and Biomembranes* 39, no. 3: 267–274. https://doi.org/10.1007/s10863-007-9086-x.

Chiu, C.-C., T.-H. Yeh, C.-S. Lu, et al. 2017. "PARK14 PLA2G6 Mutants Are Defective in Preventing Rotenone-Induced Mitochondrial Dysfunction, ROS Generation and Activation of Mitochondrial Apoptotic Pathway." *Oncotarget* 8, no. 45: 79046–79060. https://doi.org/10.18632/oncotarget.20893.

Corenblum, M., A. McRobbie-Johnson, E. Carruth, et al. 2023. "Parallel Neurodegenerative Phenotypes in Sporadic Parkinson's Disease Fibroblasts and Midbrain Dopamine Neurons." *Progress in Neurobiology* 229: 102501. https://doi.org/10.1016/j.pneurobio.2023.102501.

Cova, I., and A. Priori. 2018. "Diagnostic Biomarkers for Parkinson's Disease at a Glance: Where Are We?" *Journal of Neural Transmission* 125, no. 10: 1417–1432. https://doi.org/10.1007/s00702-018-1910-4.

Delgado-Camprubi, M., N. Esteras, M. P. Soutar, H. Plun-Favreau, and A. Y. Abramov. 2017. "Deficiency of Parkinson's Disease-Related Gene Fbxo7 Is Associated With Impaired Mitochondrial Metabolism by PARP Activation." *Cell Death and Differentiation* 24, no. 1: 120–131. https://doi.org/10.1038/cdd.2016.104.

Dey, K., M. A. Bazala, and J. Kuznicki. 2020. "Targeting Mitochondrial Calcium Pathways as a Potential Treatment Against Parkinson's Disease." *Cell Calcium* 89: 102216. https://doi.org/10.1016/j.ceca.2020.102216.

Divakaruni, A. S., A. Paradyse, D. A. Ferrick, A. N. Murphy, and M. Jastroch. 2014. "Analysis and Interpretation of Microplate-Based Oxygen Consumption and pH Data." *Methods in Enzymology* 547: 309–354. https://doi.org/10.1016/B978-0-12-801415-8.00016-3.

Duda, J., C. Pötschke, and B. Liss. 2016. "Converging Roles of Ion Channels, Calcium, Metabolic Stress, and Activity Pattern of Substantia Nigra Dopaminergic Neurons in Health and Parkinson's Disease." *Journal of Neurochemistry* 139, no. S1: 156–178. https://doi.org/10.1111/jnc.13572.

Engel, L. A., Z. Jing, D. E. O'Brien, M. Sun, and P. T. Kotzbauer. 2010. "Catalytic Function of PLA2G6 Is Impaired by Mutations Associated With Infantile Neuroaxonal Dystrophy but Not Dystonia-Parkinsonism." *PLoS One* 5, no. 9: e12897. https://doi.org/10.1371/journal.pone.0012897.

Ezeriņa, D., Y. Takano, K. Hanaoka, Y. Urano, and T. P. Dick. 2018. "N-Acetyl Cysteine Functions as a Fast-Acting Antioxidant by Triggering Intracellular H2S and Sulfane Sulfur Production." *Cell Chemical Biology* 25, no. 4: 447–459.e4. https://doi.org/10.1016/j.chembiol.2018.01.011.

Flierl, A., L. M. A. Oliveira, L. J. Falomir-Lockhart, et al. 2014. "Higher Vulnerability and Stress Sensitivity of Neuronal Precursor Cells Carrying an Alpha-Synuclein Gene Triplication." *PLoS One* 9, no. 11: e112413. https://doi.org/10.1371/journal.pone.0112413.

Folmes, C. D. L., T. J. Nelson, A. Martinez-Fernandez, et al. 2011. "Somatic Oxidative Bioenergetics Transitions Into Pluripotency-Dependent Glycolysis to Facilitate Nuclear Reprogramming." *Cell Metabolism* 14, no. 2: 264–271. https://doi.org/10.1016/j.cmet.2011.06.011.

Frank, M., S. Duvezin-Caubet, S. Koob, et al. 2012. "Mitophagy Is Triggered by Mild Oxidative Stress in a Mitochondrial Fission Dependent Manner." *Biochimica et Biophysica Acta (BBA) – Molecular Cell Research* 1823, no. 12: 2297–2310. https://doi.org/10.1016/j.bbamcr.2012.08.007.

Gandhi, S., A. Wood-Kaczmar, Z. Yao, et al. 2009. "PINK1-Associated Parkinson's Disease Is Caused by Neuronal Vulnerability to Calcium-Induced Cell Death." *Molecular Cell* 33, no. 5: 627–638. https://doi.org/10.1016/j.molcel.2009.02.013.

Ganley, I. G., P.-M. Wong, N. Gammoh, and X. Jiang. 2011. "Distinct Autophagosomal-Lysosomal Fusion Mechanism Revealed by Thapsigargin-Induced Autophagy Arrest." *Molecular Cell* 42, no. 6: 731–743. https://doi.org/10.1016/j.molcel.2011.04.024.

Gopurappilly, R. 2021. "Pluripotent Stem Cell Derived Neurons as in Vitro Models for Studying Autosomal Recessive Parkinson's Disease (ARPD): PLA2G6 and Other Gene Loci." In *Cell Biology and Translational Medicine, Volume 14: Stem Cells in Lineage Specific Differentiation and Disease*, edited by K. Turksen, 115–133. Springer International Publishing. https://doi.org/10.1007/5584_2021_643.

Gopurappilly, R., B. K. Deb, P. Chakraborty, and G. Hasan. 2018. "Stable STIM1 Knockdown in Self-Renewing Human Neural Precursors Promotes Premature Neural Differentiation." *Frontiers in Molecular Neuroscience* 11. https://doi.org/10.3389/fnmol.2018.00178.

Gopurappilly, R., B. K. Deb, P. Chakraborty, and G. Hasan. 2019. "Measurement of Store-Operated Calcium Entry in Human Neural Cells: From Precursors to Differentiated Neurons." *Methods in Molecular Biology* 2029: 257–271. https://doi.org/10.1007/978-1-4939-9631-5_20.

Gopurappilly, R., T. Musthafa, S. Sukumaran, B. Viswanath, and G. Hasan. 2023. "Generation of Feeder-Independent Transgene-Free iPSC Lines From a Young-Onset Parkinson's Disease (YOPD) Patient With a Homozygous PLA2G6: C.2222G>A (p. Arg741Gln) Mutation (NCBSi003-A) and Unaffected Heterozygous Parent (NCBSi004-A)." *Stem Cell Research* 67: 103033. https://doi.org/10.1016/j.scr.2023.103033.

Grace, A., and S. Onn. 1989. "Morphology and Electrophysiological Properties of Immunocytochemically Identified Rat Dopamine Neurons Recorded In Vitro." *Journal of Neuroscience* 9, no. 10: 3463–3481. https://doi.org/10.1523/JNEUROSCI.09-10-03463.1989.

Gregory, A., M. A. Kurian, E. R. Maher, P. Hogarth, and S. J. Hayflick. 1993. "PLA2G6-Associated Neurodegeneration." In *GeneReviews®*. http://www.ncbi.nlm.gov/books/NBK1675/ [Book Accession].

Grünewald, A., K. R. Kumar, and C. M. Sue. 2019. "New Insights Into the Complex Role of Mitochondria in Parkinson's Disease." *Progress in Neurobiology* 177: 73–93. https://doi.org/10.1016/j.pneurobio.2018.09.003.

Grünewald, A., L. Voges, A. Rakovic, et al. 2010. "Mutant Parkin Impairs Mitochondrial Function and Morphology in Human Fibroblasts." *PLoS One* 5, no. 9: e12962. https://doi.org/10.1371/journal.pone.0012962.

Gunter, T. E., L. Buntinas, G. Sparagna, R. Eliseev, and K. Gunter. 2000. "Mitochondrial Calcium Transport: Mechanisms and Functions." *Cell Calcium* 28, no. 5–6: 285–296. https://doi.org/10.1054/ceca.2000.0168.

Han, R., J. Liang, and B. Zhou. 2021. "Glucose Metabolic Dysfunction in Neurodegenerative Diseases—New Mechanistic Insights and the Potential of Hypoxia as a Prospective Therapy Targeting Metabolic Reprogramming." *International Journal of Molecular Sciences* 22, no. 11: 5887. https://doi.org/10.3390/ijms22115887.

Hekselman, I., and E. Yeger-Lotem. 2020. "Mechanisms of Tissue and Cell-Type Specificity in Heritable Traits and Diseases." *Nature Reviews Genetics* 21, no. 3: 137–150. https://doi.org/10.1038/s41576-019-0200-9.

Henrich, M. T., W. H. Oertel, D. J. Surmeier, and F. F. Geibl. 2023. "Mitochondrial Dysfunction in Parkinson's Disease – A Key Disease Hallmark With Therapeutic Potential." *Molecular Neurodegeneration* 18, no. 1: 83. https://doi.org/10.1186/s13024-023-00676-7.

Hou, X., J. O. Watzlawik, F. C. Fiesel, and W. Springer. 2020. "Autophagy in Parkinson's Disease." *Journal of Molecular Biology* 432, no. 8: 2651–2672. https://doi.org/10.1016/j.jmb.2020.01.037.

Hu, Q., and G. Wang. 2016. "Mitochondrial Dysfunction in Parkinson's Disease." *Translational Neurodegeneration* 5, no. 1: 14. https://doi.org/10.1186/s40035-016-0060-6.

Iliadi, K. G., O. B. Gluscencova, N. Iliadi, and G. L. Boulianne. 2018. "Mutations in the Drosophila Homolog of Human PLA2G6 Give Rise to Age-Dependent Loss of Psychomotor Activity and Neurodegeneration." *Scientific Reports* 8, no. 1: 2939. https://doi.org/10.1038/s41598-018-21343-8.

Imaizumi, Y., Y. Okada, W. Akamatsu, et al. 2012. "Mitochondrial Dysfunction Associated With Increased Oxidative Stress and α-Synuclein Accumulation in PARK2 iPSC-Derived Neurons and Postmortem Brain Tissue." *Molecular Brain* 5, no. 1: 35. https://doi.org/10.1186/1756-6606-5-35.

Jin, S. M., M. Lazarou, C. Wang, L. A. Kane, D. P. Narendra, and R. J. Youle. 2010. "Mitochondrial Membrane Potential Regulates PINK1 Import and Proteolytic Destabilization by PARL." *Journal of Cell Biology* 191, no. 5: 933–942. https://doi.org/10.1083/jcb.201008084.

Joselin, A. P., S. J. Hewitt, S. M. Callaghan, et al. 2012. "ROS-Dependent Regulation of Parkin and DJ-1 Localization During Oxidative Stress in Neurons." *Human Molecular Genetics* 21, no. 22: 4888–4903. https://doi.org/10.1093/hmg/dds325.

Ke, M., C.-M. Chong, H. Zeng, et al. 2020. "Azoramide Protects iPSC-Derived Dopaminergic Neurons With PLA2G6 D331Y Mutation Through Restoring ER Function and CREB Signaling." *Cell Death & Disease* 11, no. 2: 130. https://doi.org/10.1038/s41419-020-2312-8.

Kim, K., A. Doi, B. Wen, et al. 2010. "Epigenetic Memory in Induced Pluripotent Stem Cells." *Nature* 467, no. 7313: 285–290. https://doi.org/10.1038/nature09342.

Kinghorn, K. J., and J. I. Castillo-Quan. 2016. "Mitochondrial Dysfunction and Defects in Lipid Homeostasis as Therapeutic Targets in Neurodegeneration With Brain Iron Accumulation." *Rare Diseases* 4, no. 1: e1128616. https://doi.org/10.1080/21675511.2015.1128616.

Kinghorn, K. J., J. I. Castillo-Quan, F. Bartolome, et al. 2015. "Loss of PLA2G6 Leads to Elevated Mitochondrial Lipid Peroxidation and Mitochondrial Dysfunction." *Brain* 138, no. 7: 1801–1816. https://doi.org/10.1093/brain/awv132.

Koentjoro, B., J.-S. Park, and C. M. Sue. 2017. "Nix Restores Mitophagy and Mitochondrial Function to Protect Against PINK1/Parkin-Related Parkinson's Disease." *Scientific Reports* 7, no. 1: 44373. https://doi.org/10.1038/srep44373.

Kondapalli, C., A. Kazlauskaite, N. Zhang, et al. 2012. "PINK1 Is Activated by Mitochondrial Membrane Potential Depolarization and Stimulates Parkin E3 Ligase Activity by Phosphorylating Serine 65." *Open Biology* 2, no. 5: 120080. https://doi.org/10.1098/rsob.120080.

Kostic, M., M. H. R. Ludtmann, H. Bading, et al. 2015. "PKA Phosphorylation of NCLX Reverses Mitochondrial Calcium Overload and Depolarization, Promoting Survival of PINK1-Deficient Dopaminergic Neurons." *Cell Reports* 13, no. 2: 376–386. https://doi.org/10.1016/j.celrep.2015.08.079.

Lesage, S., V. Drouet, E. Majounie, et al. 2016. "Loss of VPS13C Function in Autosomal-Recessive Parkinsonism Causes Mitochondrial Dysfunction and Increases PINK1/Parkin-Dependent Mitophagy." *American Journal of Human Genetics* 98, no. 3: 500–513. https://doi.org/10.1016/j.ajhg.2016.01.014.

Lewis, R. S. 2020. "Store-Operated Calcium Channels: From Function to Structure and Back Again." *Cold Spring Harbor Perspectives in Biology* 12, no. 5: a035055. https://doi.org/10.1101/cshperspect.a035055.

Liang, K. X., C. K. Kristiansen, S. Mostafavi, et al. 2020. "Disease-Specific Phenotypes in iPSC -Derived Neural Stem Cells With POLG Mutations." *EMBO Molecular Medicine* 12, no. 10: e12146. https://doi.org/10.15252/emmm.202012146.

Lin, G., P.-T. Lee, K. Chen, et al. 2018. "Phospholipase PLA2G6, a Parkinsonism-Associated Gene, Affects Vps26 and Vps35, Retromer Function, and Ceramide Levels, Similar to α-Synuclein Gain." *Cell Metabolism* 28, no. 4: 605–618. https://doi.org/10.1016/j.cmet.2018.05.019.

Liu, J., J. Tan, B. Tang, and J. Guo. 2024. "Unveiling the Role of iPLA2β in Neurodegeneration: From Molecular Mechanisms to Advanced Therapies." *Pharmacological Research* 202: 107114. https://doi.org/10.1016/j.phrs.2024.107114.

Ludtmann, M. H. R., and A. Y. Abramov. 2018. "Mitochondrial Calcium Imbalance in Parkinson's Disease." *Neuroscience Letters* 663: 86–90. https://doi.org/10.1016/j.neulet.2017.08.044.

Magrinelli, F., S. Mehta, G. Di Lazzaro, et al. 2022. "Dissecting the Phenotype and Genotype of PLA2G6-Related Parkinsonism." *Movement Disorders* 37, no. 1: 148–161. https://doi.org/10.1002/mds.28807.

Malley, K. R., O. Koroleva, I. Miller, et al. 2018. "The Structure of iPLA2β Reveals Dimeric Active Sites and Suggests Mechanisms of Regulation and Localization." *Nature Communications* 9, no. 1: 765. https://doi.org/10.1038/s41467-018-03193-0.

Marchetti, P., Q. Fovez, N. Germain, R. Khamari, and J. Kluza. 2020. "Mitochondrial Spare Respiratory Capacity: Mechanisms, Regulation, and Significance in Non-Transformed and Cancer Cells." *FASEB Journal* 34, no. 10: 13106–13124. https://doi.org/10.1096/fj.202000767R.

Matteucci, A., M. Patron, D. Vecellio Reane, et al. 2018. "Parkin-Dependent Regulation of the MCU Complex Component MICU1." *Scientific Reports* 8, no. 1: 14199. https://doi.org/10.1038/s41598-018-32551-7.

Mizushima, N., and T. Yoshimori. 2007. "How to Interpret LC3 Immunoblotting." *Autophagy* 3, no. 6: 542–545. https://doi.org/10.4161/auto.4600.

Morais, V. A., D. Haddad, K. Craessaerts, et al. 2014. "PINK1 Loss-Of-Function Mutations Affect Mitochondrial Complex I Activity via NdufA10 Ubiquinone Uncoupling." *Science* 344, no. 6180: 203–207. https://doi.org/10.1126/science.1249161.

Mori, A., T. Hatano, T. Inoshita, et al. 2019. "Parkinson's Disease-Associated iPLA2-VIA/PLA2G6 Regulates Neuronal Functions and α-Synuclein Stability Through Membrane Remodeling." *Proceedings of the National Academy of Sciences* 116, no. 41: 20689–20699. https://doi.org/10.1073/pnas.1902958116.

Mytilineou, C., P. Werner, S. Molinari, A. Rocco, G. Cohen, and M. D. Yahr. 1994. "Impaired Oxidative Decarboxylation of Pyruvate in Fibroblasts From Patients With Parkinson's Disease." *Journal of Neural Transmission – Parkinson's Disease and Dementia Section* 8, no. 3: 223–228. https://doi.org/10.1007/BF02260943.

Narendra, D. P., and R. J. Youle. 2024. "The Role of PINK1–Parkin in Mitochondrial Quality Control." *Nature Cell Biology* 26, no. 10: 1639–1651. https://doi.org/10.1038/s41556-024-01513-9.

Nechushtai, L., D. Frenkel, and R. Pinkas-Kramarski. 2023. "Autophagy in Parkinson's Disease." *Biomolecules* 13, no. 10: 1435. https://doi.org/10.3390/biom13101435.

Newington, J. T., A. Pitts, A. Chien, R. Arseneault, D. Schubert, and R. C. Cumming. 2011. "Amyloid Beta Resistance in Nerve Cell Lines Is Mediated by the Warburg Effect." *PLoS One* 6, no. 4: e19191. https://doi.org/10.1371/journal.pone.0019191.

Palacino, J. J., D. Sagi, M. S. Goldberg, et al. 2004. "Mitochondrial Dysfunction and Oxidative Damage in Parkin-Deficient Mice." *Journal of Biological Chemistry* 279, no. 18: 18614–18622. https://doi.org/10.1074/jbc.M401135200.

Panopoulos, A. D., O. Yanes, S. Ruiz, et al. 2012. "The Metabolome of Induced Pluripotent Stem Cells Reveals Metabolic Changes Occurring in Somatic Cell Reprogramming." *Cell Research* 22, no. 1: 168–177. https://doi.org/10.1038/cr.2011.177.

Parekh, A. B., and J. W. Putney. 2005. "Store-Operated Calcium Channels." *Physiological Reviews* 85, no. 2: 757–810. https://doi.org/10.1152/physrev.00057.2003.

Pathak, T., T. Agrawal, S. Richhariya, S. Sadaf, and G. Hasan. 2015. "Store-Operated Calcium Entry Through Orai Is Required for Transcriptional Maturation of the Flight Circuit in Drosophila." *Journal of Neuroscience* 35, no. 40: 13784–13799. https://doi.org/10.1523/JNEUROSCI.1680-15.2015.

Pedre, B., U. Barayeu, D. Ezeriņa, and T. P. Dick. 2021. "The Mechanism of Action of N-Acetylcysteine (NAC): The Emerging Role of H2S and Sulfane Sulfur Species." *Pharmacology & Therapeutics* 228: 107916. https://doi.org/10.1016/j.pharmthera.2021.107916.

Perier, C., and M. Vila. 2012. "Mitochondrial Biology and Parkinson's Disease." *Cold Spring Harbor Perspectives in Medicine* 2, no. 2: a009332. https://doi.org/10.1101/cshperspect.a009332.

Pissadaki, E. K., and J. P. Bolam. 2013. "The Energy Cost of Action Potential Propagation in Dopamine Neurons: Clues to Susceptibility in Parkinson's Disease." *Frontiers in Computational Neuroscience* 7: 13. https://doi.org/10.3389/fncom.2013.00013.

Polo, J. M., S. Liu, M. E. Figueroa, et al. 2010. "Cell Type of Origin Influences the Molecular and Functional Properties of Mouse Induced Pluripotent Stem Cells." *Nature Biotechnology* 28, no. 8: 848–855. https://doi.org/10.1038/nbt.1667.

Prakriya, M., and R. S. Lewis. 2015. "Store-Operated Calcium Channels." *Physiological Reviews* 95, no. 4: 1383–1436. https://doi.org/10.1152/physrev.00020.2014.

Putney, J. W., N. Steinckwich-Besançon, T. Numaga-Tomita, et al. 2017. "The Functions of Store-Operated Calcium Channels." *Biochimica et Biophysica Acta (BBA) – Molecular Cell Research* 1864, no. 6: 900–906. https://doi.org/10.1016/j.bbamcr.2016.11.028.

Qadri, R., M. Namdeo, M. Behari, V. Goyal, S. Sharma, and A. K. Mukhopadhyay. 2018. "Alterations in Mitochondrial Membrane Potential in Peripheral Blood Mononuclear Cells in Parkinson's Disease: Potential for a Novel Biomarker." *Restorative Neurology and Neuroscience* 36, no. 6: 719–727. https://doi.org/10.3233/RNN-180852.

Rakovic, A., A. Grunewald, P. Seibler, et al. 2010. "Effect of Endogenous Mutant and Wild-Type PINK1 on Parkin in Fibroblasts From Parkinson Disease Patients." *Human Molecular Genetics* 19, no. 16: 3124–3137. https://doi.org/10.1093/hmg/ddq215.

Risiglione, P., F. Zinghirino, M. C. Di Rosa, A. Magrì, and A. Messina. 2021. "Alpha-Synuclein and Mitochondrial Dysfunction in Parkinson's Disease: The Emerging Role of VDAC." *Biomolecules* 11, no. 5: 718. https://doi.org/10.3390/biom11050718.

Rothfuss, O., H. Fischer, T. Hasegawa, et al. 2009. "Parkin Protects Mitochondrial Genome Integrity and Supports Mitochondrial DNA Repair." *Human Molecular Genetics* 18, no. 20: 3832–3850. https://doi.org/10.1093/hmg/ddp327.

Scorziello, A., D. Borzacchiello, M. J. Sisalli, R. Di Martino, M. Morelli, and A. Feliciello. 2020. "Mitochondrial Homeostasis and Signaling in Parkinson's Disease." *Frontiers in Aging Neuroscience* 12: 100. https://doi.org/10.3389/fnagi.2020.00100.

Smith, A. M., C. Depp, B. J. Ryan, et al. 2018. "Mitochondrial Dysfunction and Increased Glycolysis in Prodromal and Early Parkinson's Blood Cells." *Movement Disorders* 33, no. 10: 1580–1590. https://doi.org/10.1002/mds.104.

Smith, G. A., J. Jansson, E. M. Rocha, T. Osborn, P. J. Hallett, and O. Isacson. 2016. "Fibroblast Biomarkers of Sporadic Parkinson's Disease and LRRK2 Kinase Inhibition." *Molecular Neurobiology* 53, no. 8: 5161–5177. https://doi.org/10.1007/s12035-015-9435-4.

Stevens, D. A., Y. Lee, H. C. Kang, et al. 2015. "Parkin Loss Leads to PARIS-Dependent Declines in Mitochondrial Mass and Respiration." *Proceedings of the National Academy of Sciences* 112, no. 37: 11696–11701. https://doi.org/10.1073/pnas.1500624112.

Strokin, M., and G. Reiser. 2016. "Mitochondria From a Mouse Model of the Human Infantile Neuroaxonal Dystrophy (INAD) With Genetic Defects in VIA iPLA 2 Have Disturbed Ca2+ Regulation With Reduction in Ca2+ Capacity." *Neurochemistry International* 99: 187–193. https://doi.org/10.1016/j.neuint.2016.07.002.

Sun, W.-Y., V. A. Tyurin, K. Mikulska-Ruminska, et al. 2021. "Phospholipase iPLA2β Averts Ferroptosis by Eliminating a Redox Lipid Death Signal." *Nature Chemical Biology* 17, no. 4: 465–476. https://doi.org/10.1038/s41589-020-00734-x.

Surmeier, D. J., J. N. Guzman, J. Sanchez, and P. T. Schumacker. 2012. "Physiological Phenotype and Vulnerability in Parkinson's Disease." *Cold Spring Harbor Perspectives in Medicine* 2, no. 7: a009290. https://doi.org/10.1101/cshperspect.a009290.

Tang, B. L. 2020. "Glucose, Glycolysis, and Neurodegenerative Diseases." *Journal of Cellular Physiology* 235, no. 11: 7653–7662. https://doi.org/10.1002/jcp.29682.

Tang, J., R. W. Kriz, N. Wolfman, M. Shaffer, J. Seehra, and S. S. Jones. 1997. "A Novel Cytosolic Calcium-Independent Phospholipase A2 Contains Eight Ankyrin Motifs." *Journal of Biological Chemistry* 272, no. 13: 8567–8575. https://doi.org/10.1074/jbc.272.13.8567.

Tanida, I., T. Nishitani, T. Nemoto, T. Ueno, and E. Kominami. 2002. "Mammalian Apg12p, but Not the Apg12p · Apg5p Conjugate, Facilitates LC3 Processing." *Biochemical and Biophysical Research Communications* 296, no. 5: 1164–1170. https://doi.org/10.1016/S0006-291X(02)02057-0.

Tanida, I., T. Ueno, and E. Kominami. 2004. "LC3 Conjugation System in Mammalian Autophagy." *International Journal of Biochemistry & Cell Biology* 36, no. 12: 2503–2518. https://doi.org/10.1016/j.biocel.2004.05.009.

Trist, B. G., D. J. Hare, and K. L. Double. 2019. "Oxidative Stress in the Aging Substantia Nigra and the Etiology of Parkinson's Disease." *Aging Cell* 18, no. 6: e13031. https://doi.org/10.1111/acel.13031.

van der Merwe, C., B. Loos, C. Swart, et al. 2014. "Mitochondrial Impairment Observed in Fibroblasts From South African Parkinson's Disease Patients With Parkin Mutations." *Biochemical and Biophysical Research Communications* 447, no. 2: 334–340. https://doi.org/10.1016/j.bbrc.2014.03.151.

Vig, M., C. Peinelt, A. Beck, et al. 2006. "CRACM1 Is a Plasma Membrane Protein Essential for Store-Operated Ca^{2+} Entry." *Science* 312, no. 5777: 1220–1223. https://doi.org/10.1126/science.1127883.

Villalón-García, I., M. Álvarez-Córdoba, S. Povea-Cabello, et al. 2022. "Vitamin E Prevents Lipid Peroxidation and Iron Accumulation in PLA2G6-Associated Neurodegeneration." *Neurobiology of Disease* 165: 105649. https://doi.org/10.1016/j.nbd.2022.105649.

Wang, H.-L., A.-H. Chou, A.-S. Wu, et al. 2011. "PARK6 PINK1 Mutants Are Defective in Maintaining Mitochondrial Membrane Potential and Inhibiting ROS Formation of Substantia Nigra Dopaminergic Neurons." *Biochimica et Biophysica Acta (BBA) – Molecular Basis of Disease* 1812, no. 6: 674–684. https://doi.org/10.1016/j.bbadis.2011.03.007.

Wei, H., L. Liu, and Q. Chen. 2015. "Selective Removal of Mitochondria via Mitophagy: Distinct Pathways for Different Mitochondrial Stresses." *Biochimica et Biophysica Acta (BBA) – Molecular Cell Research* 1853, no. 10: 2784–2790. https://doi.org/10.1016/j.bbamcr.2015.03.013.

Winkler-Stuck, K., F. R. Wiedemann, C.-W. Wallesch, and W. S. Kunz. 2004. "Effect of Coenzyme Q10 on the Mitochondrial Function of Skin Fibroblasts From Parkinson Patients." *Journal of the Neurological Sciences* 220, no. 1–2: 41–48. https://doi.org/10.1016/j.jns.2004.02.003.

Wolf, M. J., and R. W. Gross. 1996. "Expression, Purification, and Kinetic Characterization of a Recombinant 80-kDa Intracellular Calcium-Independent Phospholipase A2." *Journal of Biological Chemistry* 271, no. 48: 30879–30885. https://doi.org/10.1074/jbc.271.48.30879.

Xiao, B., J.-Y. Goh, L. Xiao, H. Xian, K.-L. Lim, and Y.-C. Liou. 2017. "Reactive Oxygen Species Trigger Parkin/PINK1 Pathway–Dependent Mitophagy by Inducing Mitochondrial Recruitment of Parkin." *Journal of Biological Chemistry* 292, no. 40: 16697–16708. https://doi.org/10.1074/jbc.M117.787739.

Xiao, B., J. Kuruvilla, and E.-K. Tan. 2022. "Mitophagy and Reactive Oxygen Species Interplay in Parkinson's Disease." *NPJ Parkinson's Disease* 8, no. 1: 135. https://doi.org/10.1038/s41531-022-00402-y.

Yadava, N., and D. G. Nicholls. 2007. "Spare Respiratory Capacity Rather Than Oxidative Stress Regulates Glutamate Excitotoxicity After Partial Respiratory Inhibition of Mitochondrial Complex I With Rotenone." *Journal of Neuroscience* 27, no. 27: 7310–7317. https://doi.org/10.1523/JNEUROSCI.0212-07.2007.

Yakhine-Diop, S. M. S., J. M. Bravo-San Pedro, R. Gómez-Sánchez, et al. 2014. "G2019S LRRK2 Mutant Fibroblasts From Parkinson's Disease Patients Show Increased Sensitivity to Neurotoxin 1-Methyl-4-Phenylpyridinium Dependent of Autophagy." *Toxicology* 324: 1–9. https://doi.org/10.1016/j.tox.2014.07.001.

Yamamoto-Imoto, H., E. Hara, S. Nakamura, and T. Yoshimori. 2022. "Measurement of Autophagy via LC3 Western Blotting Following DNA-Damage-Induced Senescence." *STAR Protocols* 3, no. 3: 101539. https://doi.org/10.1016/j.xpro.2022.101539.

Yoshimori, T., A. Yamamoto, Y. Moriyama, M. Futai, and Y. Tashiro. 1991. "Bafilomycin A1, a Specific Inhibitor of Vacuolar-Type H(+)-ATPase, Inhibits Acidification and Protein Degradation in Lysosomes of Cultured Cells." *Journal of Biological Chemistry* 266, no. 26: 17707–17712. https://doi.org/10.1016/S0021-9258(19)47429-2.

Youle, R. J., and D. P. Narendra. 2011. "Mechanisms of Mitophagy." *Nature Reviews Molecular Cell Biology* 12, no. 1: 9–14. https://doi.org/10.1038/nrm3028.

Zaltieri, M., F. Longhena, M. Pizzi, C. Missale, P. Spano, and A. Bellucci. 2015. "Mitochondrial Dysfunction and α-Synuclein Synaptic Pathology in Parkinson's Disease: Who's on First?" *Parkinson's Disease* 2015: 1–10. https://doi.org/10.1155/2015/108029.

Zambon, F., M. Cherubini, H. J. R. Fernandes, et al. 2019. "Cellular α-Synuclein Pathology Is Associated With Bioenergetic Dysfunction in Parkinson's iPSC-Derived Dopamine Neurons." *Human Molecular Genetics* 28, no. 12: 2001–2013. https://doi.org/10.1093/hmg/ddz038.

Zampese, E., and D. J. Surmeier. 2020. "Calcium, Bioenergetics, and Parkinson's Disease." *Cells* 9, no. 9: 2045. https://doi.org/10.3390/cells9092045.

Zanellati, M. C., V. Monti, C. Barzaghi, et al. 2015. "Mitochondrial Dysfunction in Parkinson Disease: Evidence in Mutant PARK2 Fibroblasts." *Frontiers in Genetics* 6. https://doi.org/10.3389/fgene.2015.00078.

Zhang, C., M. Lin, R. Wu, et al. 2011. "Parkin, a p53 Target Gene, Mediates the Role of p53 in Glucose Metabolism and the Warburg Effect." *Proceedings of the National Academy of Sciences* 108, no. 39: 16259–16264. https://doi.org/10.1073/pnas.1113884108.

Zhou, Q., A. Yen, G. Rymarczyk, et al. 2016. "Impairment of PARK14-Dependent Ca2+ Signalling Is a Novel Determinant of Parkinson's Disease." *Nature Communications* 7, no. 1: 10332. https://doi.org/10.1038/ncomms10332.

Zorov, D. B., M. Juhaszova, and S. J. Sollott. 2014. "Mitochondrial Reactive Oxygen Species (ROS) and ROS-Induced ROS Release." *Physiological Reviews* 94, no. 3: 909–950. https://doi.org/10.1152/physrev.00026.2013.

Supporting Information

Additional supporting information can be found online in the Supporting Information section.